The origin of Halley-type comets: probing the inner Oort cloud

Harold F. Levison
Department of Space Studies, Southwest Research Institute, Boulder, CO 80302

Luke Dones
Department of Space Studies, Southwest Research Institute, Boulder, CO 80302

and

Martin J. Duncan
Department of Physics, Queen's University, Kingston, Ontario, Canada K7L 3N6

ABSTRACT

We have integrated the orbits of 27,700 test particles initially entering the planetary system from the Oort cloud in order to study the origin of Halley-type comets (HTCs). We included the gravitational influence of the Sun, giant planets, passing stars, and galactic tides. We find that an isotropically distributed Oort cloud does not reproduce the observed orbital element distribution of the HTCs. In order to match the observations, the initial inclination distribution of the progenitors of the HTCs must be similar to the observed HTC inclination distribution. We can match the observations with an Oort cloud that consists of an isotropic outer cloud and a disk-like massive inner cloud. These idealized two-component models have inner disks with median inclinations that range from 10 to 50°. This analysis represents the first link between observations and the structure of the inner Oort cloud.

Subject headings: comets: general; solar system: formation; solar system: general; Kuiper Belt, Oort cloud

1. Introduction

The structure of the Oort cloud, particularly the inner Oort cloud, represents a vital clue to the formation of the Solar System. The number and orbital element distribution of comets in the Oort cloud was determined by the planet formation process as well as the environment in which the Solar System formed (for example see Gaidos 1995, Fernández 1997). Thus, understanding the structure of the Oort cloud would put important constraints on models of Solar System formation.

A full understanding of the Oort cloud cannot be determined by the study of long-period comets alone. These comets, which evolve directly from the Oort cloud to the inner Solar System, come from a region of the Oort cloud beyond $10,000 - 20,000$ AU where galactic tides are strong enough that a comet's perihelion distance can evolve from $q > 30\,AU$ to $q \lesssim 1.5\,AU$ in just one orbital period (Hills 1981; Duncan, Quinn, & Tremaine 1987 [hereafter DQT87]). Objects interior to $10,000$ AU very rarely make it directly into the inner Solar System. However, these objects are slowly leaking into the realm of the giant planets. Numerical simulations (Duncan, Quinn, & Tremaine 1988; Quinn, Tremaine, & Duncan 1990 [hereafter DQT88 and QTD90, respectively]; Emel'yanenko & Bailey 1998 [hereafter EB98]) show that these objects are an important source of Halley-type comets (those comets with orbit periods less than 200 years and with Tisserand parameters with respect to Jupiter, T, less than 2; Carusi et al. [1987]; Levison [1996]). Thus, Halley-type comets (hereafter HTCs) may represent our only observable link to the inner Oort cloud.

The only works of which we are aware that study the origin of Halley-type comets are DQT88, QTD90, and EB98. (Wiegert & Tremaine [1999] recently studied the evolution of comets in the Oort cloud, but they followed too few objects to generate a population of HTCs large enough to be usefully studied.) DQT88 and later QTD90 studied the origin of the short-period comets in general, but they were mainly interested in the Jupiter-family comets (short-period comets with $T > 2$, hereafter referred to as JFCs). They showed that it is not possible to reproduce the very narrow inclination distribution of the JFCs from the isotropically distributed Oort cloud comets. Indeed, the source region must be a disk, i.e. the Kuiper belt. On the other hand, QTD90 concluded that the HTCs, being more isotropic than the JFCs, did indeed originate in the Oort cloud. Thus, the popular wisdom for nearly a decade has been that JFCs originated in the Kuiper belt (or now perhaps the scattered disk; see Duncan & Levison 1997), while the HTCs were captured Oort cloud comets (see Levison 1996 for a review).

However, a reanalysis of QTD90's results shows that while their integrations do reproduce the Jupiter family from the Kuiper Belt fairly well, they do not adequately produce the HTCs from the Oort Cloud. This is illustrated in figure 1, which compares the orbital

element distribution of the known HTCs (the solid curve) and QTD90's HTC model (the dotted curve). Figures 1a and 1b show the cumulative semi-major axis and inclination distributions. Only objects with perihelion distances, q, less than 1.5 AU are plotted to attempt to correct for observational incompleteness. The two distributions are significantly different. For example, only $\sim 21\%$ of the HTCs in our solar system have semi-major axes inside the orbit of Saturn, while QTD90's simulation predicts that 64% of all HTCs should lie there. In addition, QTD90's simulation predicts an isotropic inclination distribution for the HTCs, while the observed distribution has a median inclination of only 45°. QTD90 predicts a significant population of HTCs with high inclinations and small semi-major axes that does not appear to exist in nature. (Since the 'missing' comets have semi-major axes that are smaller than the observed objects, they cannot be explained away by observational biases.)

While ambitious for its time, QTD90 had to make some very significant simplifications in order to perform their simulations. They increased the masses of the planets by at least a factor of 10 so that their comets would dynamically evolve faster. In addition, they started their 'Oort cloud' comets with a semi-major axis of only $50\,AU$ in order to increase the capture probability. Either of these simplifications could explain the discrepancies noted in Figure 1. Unfortunately, EB98's simulations cannot be used to address these discrepancies, because they almost totally ignored the inner Oort cloud and do not discuss the orbital element distribution of their synthetic HTCs.

One possible solution to the above problem is that some of the low inclination HTCs could actually originate in the Kuiper belt. This issue was addressed in detail in Levison & Duncan (1997), where, using numerical integrations, they followed the trajectories of objects from the Kuiper belt. Considering those objects with instantaneous semi-major axes inside of 30AU and instantaneous perihelion distances less than 2.5AU, they found that in steady state roughly 13% of them were Halley-type comets ($T < 2$). Since the ratio of the number of HTCs to Jupiter-family comets (JFCs) is roughly this number, at first glance the Kuiper belt looks like a possible solution to the HTC inclination-distribution problem. Unfortunately, the orbital element distribution of the HTCs produced in Levison & Duncan's simulation is significantly different than that observed in nature (see Levison & Duncan for a discussion). For example, they all had low inclinations. Levison & Duncan also note that 1) all the HTCs in their simulation were first JFCs, and 2) it takes at least 10^5 years and usually over 10^6 years to become a visible HTC after the comet first becomes visible as a JFC. Levison & Duncan therefore conclude that the objects from the Kuiper belt become extinct before they become HTCs. Thus, they conclude that the Kuiper belt is not an important source of active HTCs. However, the integrations of Levison & Duncan (1997) assumed dynamically cold initial conditions with inclinations less than 25°. We now know that the Kuiper Belt and scattered disk (Duncan & Levison 1997) contain objects with inclinations as high as 40°.

Although we do not believe that the inclusion of the high inclination objects will significantly affect the above conclusions, in future work we will consider a dynamically hot Kuiper Belt as a possible source region for HTCs.

Here we present the results of a numerical integration of the capture of Oort cloud comets into HTC orbits using modern techniques that do not require the simplifications used in QTD90. Our goal is to supply constraints on the structure of the Oort cloud by forcing our models to match the observed distribution of HTCs (corrected for observational biases). In §2, we describe the methods used in these simulations as well as how we generated the initial conditions. In §3 we describe the results of the integrations. In §4 we describe our one-component model of the Oort cloud, and in §5 we describe our two-component model. Finally, our conclusions are presented in §6.

2. Numerical Methods and Initial Conditions

In our simulations Oort cloud comets were treated as massless test particles. Since we do not know the structure of the inner Oort cloud, we generated the initial conditions for the particles using the following methods. In §4 and §5, we will adjust the structure of the Oort cloud by applying different weights to these particles. In this way, we can study how the structure of the Oort cloud affects our results without performing a large number of separate integrations.

The probability that a particle gets captured into a HTC-like orbit is strongly dependent on its initial orbital elements. We wanted to insure that our results were not affected by small number statistics or that we did not discount the importance of a region of the Oort cloud because no particles were captured. So, we divided the Oort cloud into 36 bins in a–i–q space and we put more particles in the bins with a small capture probability. In particular, the semi-major axis (a_0), which extended from 5000 AU to 50,000 AU, was divided into three bins with boundaries at 10,000 AU and 25,000 AU. The inclination (i_0) was also divided into 3 bins with boundaries at 60° and 100°. Finally, the perihelion distance (q_0) was divided into 4 bins with boundaries at 5 AU, 10 AU, and 20 AU.

Within each bin the orbital elements of the test particles were initially:

1. Uniformly distributed in semi-major axis.

2. Uniformly distributed in perihelion distance from q_{min} to the outer bin boundary. The value of q_{min} is defined as follows. The overall perihelion distribution is uniform in q with an inner edge intended to mimic the so-called 'Jupiter barrier' which constrains any small perihelion, dynamically new long-period comet (hereafter LPC) to have $a \gtrsim 20,000$ AU (Hills 1981). The basic idea is that dynamically new LPCs must have had $q > q_i \sim 10$ AU the last time through perihelion. (If not, the comet would have received a kick comparable to its binding energy.) If we define Δq as the expected change in the perihelion distance of an object in one orbital period due to galactic tides, then $(q_i - \Delta q)$ is the smallest perihelion distance that we expect a dynamically new LPC to have. Following DQT87, the typical change in a comet's perihelion distance, q, in time t is approximately

$$\Delta q \approx \frac{1}{\sqrt{G\,M_\odot}} 5\pi G \rho_\circ q^{1/2} a^2 t \sin^2 i, \tag{1}$$

where $M_\odot$ is the mass of the Sun, $\rho_\circ$ is the mean density of the galactic disk, and a and i are the comet's semi-major axis and inclination with respect to the galactic plane, respectively. We set $\rho_\circ = 0.1\,M_\odot/pc^3$ (we justify this value below) and $i = 120°$, which

is the inclination of the galactic plane with respect to the ecliptic. We also set t equal to the orbital period of the comet. So, we define the inner edge of the overall distribution as the maximum of 0.1 AU and $(q_i - \Delta q)$. Figure 2 shows $(q_i - \Delta q)$, with $q_i = 10\,\mathrm{AU}$. Note that this model predicts that we should only see dynamically new LPCs with $a > 28,000\,\mathrm{AU}$, while they are observed to have semi-major axes near $20,000\,\mathrm{AU}$. Nonetheless, we adopt this model since it is consistent with previous works. We will address the sensitivity of our results to this assumption below. For each bin, q_{min} is the larger of $(q_i - \Delta q)$ or the inner bin boundary.

3. Uniformly distributed in cosine of the inclination.

4. Uniformly distributed in argument of perihelion, ω, and longitude of the ascending node, Ω, between 0 and 2π.

5. Uniformly distributed in instantaneous heliocentric distance between 500 and 600 AU. We also required that the particles were initially moving toward the Sun. From this, we calculated the initial mean anomaly.

Initially, the relative populations of the 36 a–i–q bins also followed the above prescription. However, at the end of the initial set of integrations, we calculated the number of objects from each bin that evolved onto HTC-like orbits. We ran additional particles in those bins for which this number was smaller than 10. In total, we integrated the orbits of 27,700 test particles.

The orbit for each test particle was integrated for up to 1 billion years or until it was ejected from the system, hit the Sun or a planet, or evolved onto an orbit with $q > 45\,\mathrm{AU}$, at which point we assumed that it reentered the Oort cloud. If a particle evolved onto an orbit with $a < 100\,\mathrm{AU}$ it was cloned 19 times, by which we mean that we generated 19 new particles with positions offset from the original by a random number uniformly distributed between 0 and $10^{-7}\,\mathrm{AU}$ and with the same velocities. We followed the orbital evolution of the test particles under the gravitational effects of the Sun, giant planets, galactic tides, and passing stars using the RMVS3 integrator (Levison & Duncan 1994). RMVS3 is based on the fast N-body mapping method of Wisdom & Holman (1991). The orbits of the Sun and planets were treated as a fully interacting system. We included the effects of the passing stars using the Monte Carlo prescription developed in DQT87, which assumes the impulse approximation. Since recent work on the galactic potential seems to indicate that DQT87's galactic tide model may have been too simple, we used a more sophisticated model for these integrations.

Following Heisler & Tremaine (1986; henceforth HT86), Wiegert (1996), and Wiegert & Tremaine (1999; henceforth WT99), we assume that (1) the Galaxy is axisymmetric and (2)

the Sun follows a circular orbit of radius R_0 in the galactic midplane. The Sun's orbital speed and angular speed about the galactic center are respectively Θ_0 and Ω_0, where $\Theta_0 = \Omega_0 R_0$. We treat a comet as a massless particle orbiting in the field of the Sun, the giant planets, and the Galaxy. Consider a coordinate system centered on the moving Sun, the axes of which remain aligned with an inertial frame. In this system, the comet's equation of motion is

$$\ddot{\mathbf{r}} = \mathbf{F}_\odot + \mathbf{F}_\mathrm{p} + \mathbf{F}_\mathrm{tide}, \tag{2}$$

where $\mathbf{F}_\odot$, $\mathbf{F}_\mathrm{p}$ and $\mathbf{F}_\mathrm{tide}$ represent the accelerations due to the Sun, planets, and Galaxy respectively.

HT86 and WT99 define a rotating rectangular coordinate system $(\tilde{x}, \tilde{y}, \tilde{z})$ centered on the Sun, such that $\tilde{x}$ points away from the galactic center, $\tilde{y}$ points in the direction of the galactic rotation, and $\tilde{z}$ points toward the south[1] galactic pole. The galactic tidal acceleration is then given by

$$\mathbf{F}_\mathrm{tide} = (A-B)(3A+B)\tilde{x}\hat{\tilde{\mathbf{x}}} - (A-B)^2\tilde{y}\hat{\tilde{\mathbf{y}}} - (4\pi G\rho_0 - 2(B^2-A^2))\tilde{z}\hat{\tilde{\mathbf{z}}} \tag{3}$$

(HT86, Equation 6; Wiegert, Equation 3.22; WT99, Equation 18), where A and B are Oort's constants, ρ_0 is the density of the galactic disk in the solar neighborhood, and G is the gravitational constant. Oort's constants are defined as $A = -(\frac{R}{2}\frac{d\Omega}{dR})_{R_0}$ and $B = -(\Omega + \frac{R}{2}\frac{d\Omega}{dR})_{R_0}$, where Ω is the angular speed of galactic rotation at distance R from the galactic center. The subscript R_0 means that A and B are evaluated at $R = R_0$.

Substituting in Equation 3, we have

$$\mathbf{F}_\mathrm{tide} = -\Omega_0(\Omega_0 + 2R_0\frac{d\Omega}{dR})\tilde{x}\hat{\tilde{\mathbf{x}}} - {\Omega_0}^2\tilde{y}\hat{\tilde{\mathbf{y}}} + (-4\pi G\rho_0 + 2\Omega_0(\Omega_0 + R_0\frac{d\Omega}{dR}))\tilde{z}\hat{\tilde{\mathbf{z}}}. \tag{4}$$

If we now use $\frac{d\Omega}{dR} = \frac{1}{R}\frac{d\Theta}{dR} - \frac{\Theta}{R^2}$ and define the logarithmic derivative $\delta \equiv \frac{d\log\Theta_0}{d\log R_0} = -\frac{A+B}{A-B}$ (Matese & Whitmire 1996), we have

$$\mathbf{F}_\mathrm{tide} = \Omega_0^2[(1-2\delta)\tilde{x}\hat{\tilde{\mathbf{x}}} - \tilde{y}\hat{\tilde{\mathbf{y}}} - (\frac{4\pi G\rho_0}{\Omega_0^2} - 2\delta)\tilde{z}\hat{\tilde{\mathbf{z}}}]. \tag{5}$$

Equation 5 is identical to Equation 1 of Matese and Whitmire (1996), except that they write 2δ where we have -2δ in the coefficient of the $\hat{\tilde{\mathbf{z}}}$ term. However, this term is small and we will neglect it, as did Matese and Whitmire.

---

[1]In the standard galactic coordinate system, x points *toward* the galactic center from the Solar System barycenter; y points in the direction of galactic rotation; and z points toward the north galactic pole. It is convenient to change the coordinates so that x points *away* from the galactic center and y still points in the direction of galactic rotation. To keep the coordinate system right-handed, we must also change z so that it points toward the south galactic pole.

What values of the galactic constants should we use? Feast & Whitelock (1997) find $\Omega_0 = A - B = 27.2 \pm 0.9$ km/s/kpc, while Olling & Merrifield (1998) obtain $\Omega_0 = 25.9 \pm 1.8$ km/s/kpc. We will assume $\Omega_0 = 26$ km/s/kpc, the same value used by Heisler & Tremaine (1986).

Bahcall (1984) finds a local mass density $\rho_0 = 0.185 \pm 0.02 M_\odot/\mathrm{pc}^3$, of which 0.096 $M_\odot/\mathrm{pc}^3$ is in visible matter (stars, gas, and dust), and an almost equal amount (0.089 $M_\odot/\mathrm{pc}^3$) is in unseen matter. DQT87 used Bahcall's value of ρ_0. Recent determinations of ρ_0 using Hipparcos data have been lower by about a factor of 2. These values include $\rho_0 = 0.11 \pm 0.01 M_\odot/\mathrm{pc}^3$ (Pham 1997), $0.076 \pm 0.015 M_\odot/\mathrm{pc}^3$ (Creze et al. 1998), and $0.102 \pm 0.010 M_\odot/\mathrm{pc}^3$ (Holmberg and Flynn 2000). We will adopt $\rho_0 = 0.1 M_\odot/\mathrm{pc}^3$. (This value of ρ_0 implies that unseen matter contributes, at most, 20% of the local mass density.)

During the integrations the complete state of the system was saved every 10^4 years. In addition, if a particle had a semi-major axis less than 100 AU and a perihelion distance less than 3 AU, its orbital elements were saved once every 1000 years.

3. Raw Results

As described above, we define an HTC as a comet with orbital period $P < 200$ years and Tisserand parameter $T < 2$. Before we can make a detailed comparison between the orbital element distribution of the real HTCs and our simulated HTCs, we must first correct for the most important observational bias — the bias against the discovery of comets with large perihelion distances. Figure 3 shows the cumulative perihelion distance distribution for the real HTCs (dotted curve) and our simulated HTCs (solid curve), generated using the dataset described above with the temporal resolution of 1000 years. In the figure, the distribution of simulated comets was scaled so that the distributions had the same value at 1 AU. Figure 3 seems to indicate that the sample of observed comets is complete out to roughly $q = 1.4$ AU, but that there is significant observational incompleteness beyond this point. Thus to be conservative, in what follows we will restrict our discussion of both the real and simulated HTCs to those objects with $q < 1.3$ AU. There are 22 comets in the observed HTC population with $q < 1.3$ AU.

Figures 4A and 4B show the cumulative semi-major axis and inclination distributions for our simulated HTCs (solid) and real HTCs (dotted). The two distributions do not agree very well. Indeed, a 2-dimensional Kolmogorov-Smirnov (K-S) statistical test (Press et al. 1992) shows that the probability that the two distributions are derived from the same parent distribution is 3×10^{-5}. The largest disagreement is in the inclinations. While the median inclination of the real HTCs is only 45°, our simulated HTCs have a median inclination of 123°. Therefore, although most of the known HTCs are in prograde orbits, most of our simulated comets are on retrograde orbits.

The inclination distribution of our HTCs may seem somewhat surprising because it has been shown previously (DQT88) that the capture probability is roughly independent of inclination. Our results are consistent with this. Figure 5A shows the averaged binned probability of capture into an HTC orbit as a function of the initial inclination in the Oort cloud. The capture probability is slightly enhanced at low inclinations. In addition, there appears to be an enhancement near 120°, which is approximately the angle between the ecliptic and the galactic plane. We do not have good enough statistics to determine whether either enhancement is real. Indeed, on average the probability that a prograde object is captured onto a HTC-like orbit is $(6.0 \pm 1.0) \times 10^{-4}$, while it has a similar value of $(6.7 \pm 1.4) \times 10^{-4}$ for a retrograde object. We see a predominately retrograde population (figure 4b) because the lifetimes are different. Once an object is captured, the average length of time it survives before being removed from the system is 64,000 years for originally prograde orbits, but 102,000 years for originally retrograde orbits.

The K-S test apparently shows that the HTCs created during our simulation do not

represent the observed distribution very well. However, the comparison presented in this section does not account for various observational selection effects, the structure of the Oort cloud, or the physical evolution of the comets. In the next section, we begin to address these issues.

There are a couple of matters concerning the capture statistics that we must mention before we present our analysis below. Figure 5B shows the averaged binned probability as a function of perihelion distance. As has been seen before (Stagg & Bailey 1989; EB98), there is a strong enhancement of the probability of capture for objects with small perihelion distances. Figure 6 shows an averaged binned $\cos(i)$ for the HTCs in our simulation as a function of their initial inclinations. For reasons that we describe in detail in §5, we calculate separately these averages for objects with $a < 20,000\,\mathrm{AU}$ (filled circles) and those with $a > 20,000\,\mathrm{AU}$ (open circles). We also plotted the standard deviation within a bin for the data with $a < 20,000\,\mathrm{AU}$. Although there is a significant variation within a bin, there is a clear trend in these data. For both regions of the Oort cloud the inclination is on average conserved during the capture process. This is in agreement with earlier studies (DQT88, QTD90). With this information in hand, we now discuss the results of our modeling.

4. A One Component Oort Cloud Model

In this section we construct a model of the HTCs that begins to account for various physical aspects of the HTCs and Oort cloud. The observed distribution of the HTCs can be, and most likely is, affected by observational selection effects. Besides the observational bias against finding objects with large perihelion distances (which was accounted for above), there most likely is a bias against discovering objects with large semi-major axes and/or inclinations near 90°. In addition, comets age and become extinct. Thus, dynamically old comets are unlikely to be discovered. Another issue that we begin to address in this section is the structure of the Oort cloud itself.

To address the above issues we have constructed a series of experiments with the data described in the last section. Periodically, as we followed the trajectory of our particles, we recorded their instantaneous orbital elements. We used this data set to construct Figure 4. Here, for each entry in this data set, we calculate the likelihood that we should actually discover a comet in this orbit based on its current orbital elements and its initial orbital elements in the Oort cloud. We use the following prescription for calculating these probabilities.

As discussed above, the observed HTC population may suffer from both inclination

and semi-major axis biases. The inclination bias should be a function of $\sin(i)$ and thus is symmetric about $i = 90°$. Thus, inclination biases cannot alleviate the discrepancy in the median inclinations described above, so they are not included in our first modeling attempt. This issue is visited again below.

Since many of the HTCs have been discovered within the last few decades and HTCs can have orbital periods longer than this, the probability that a comet is discovered depends on its semi-major axis. Indeed, it is simply proportional to the probability that it has passed through perihelion during the time that the searches have been active. Thus, we define a free parameter for our model, P_{cut}, that represents this length of time (or more precisely a weighted mean of these times for various observing techniques, including corrections for sky coverage, lunar phases, cloudy weather, and the like). Thus the probability that a comet has been discovered is

$$p_P = \begin{cases} 1 & \text{if } P < P_{cut} \\ P_{cut}/P & \text{if } P > P_{cut}, \end{cases} \tag{6}$$

where P is the orbital period of the comet.

There is significant evidence that comets physically age and become extinct or disintegrate. These range from the study of individual objects like comet 107P = asteroid (4015) Wilson-Harrington (Bowell et al. 1992) to statistical arguments based on observed orbital element distributions (Weissman 1980; Levison & Duncan 1997; Wiegert & Tremaine 1999). The physical aging of a comet is usually expressed in terms of the number of perihelion passages it has undergone. Thus, we define N_q as the number of perihelion passages with $q < 2.5\,\mathrm{AU}$ that a comet undergoes before becoming extinct. This will be a free parameter in our models.

Finally, we make a first attempt at including structure in the Oort cloud. Since the observed distribution of HTCs is more prograde than predicted we flatten the initial inclination distribution. We take the probability that a particle that was in our original distribution is in our model distribution as

$$p_{i0} = \left(\frac{1}{2} + \frac{1}{2}\cos(i_0)\right)^{\gamma}, \tag{7}$$

where i_0 was the comet's initial inclination in the Oort cloud and γ is a free parameter. For convenience, we will represent this function with its median inclination, i', rather than γ. Figure 7 shows several examples of the Oort cloud inclination distributions generated by this function.

Thus our model contains three free parameters: P_{cut}, N_q, and i'. To evaluate this model, we first generate a series of predicted HTC a–i distributions for each value of these

parameters by calculating the probability, p, that each of our fictitious HTCs is in the model:

$$p = \begin{cases} p_P \times p_{i0} & \text{if comet has had fewer than } N_q \text{ perihelion passages with } q < 2.5\,\text{AU.} \\ 0 & \text{otherwise.} \end{cases} \tag{8}$$

We then construct a model using Monte Carlo techniques. Finally, we then employ the 2-dimensional K-S test to determine whether this model is a reasonable representation of the data. We chose values of P_{cut} between 20 and 200 years with a resolution of 10 years, values of N_q between 5 and 63000 with a spacing in $\log(N_q)$ of 0.3 (roughly a factor of 2), and values of i' between 10 and 90° with a spacing of 10°.

The best fit model occurs for values of $P_{cut} = 50$ years, $N_q = 8000$, and $i' = 50°$. Figure 8 compares the cumulative semi-major axis and inclination distributions of this model (solid curves) and the observed HTCs (dotted curves). There is indeed excellent agreement between the two distributions. Thus, as a first step in our analysis, we conclude that we can construct reasonable models for the HTC distribution.

We can investigate the range of good models by studying contour plots of K-S test probability, p_{KS}, as a function of our free parameters. To be precise, p_{KS} is the probability that the two populations derive from the same parent population. Figure 9 shows two slices through our 3-dimensional parameter space. These slices were chosen so that they contain our best fit model. The contours in Figure 9A show p_{KS} for our $N_q = 8000$ models as a function of i' and P_{cut}. There is a relatively sharp peak centered on our best fit model with a rapid falloff with both i' and P_{cut}. Other slices at different N_q look similar to this plot, but the center of the peak is a function of N_q. For small values of N_q the peak is further to the left on the diagram. Also the height of the peak decreases with smaller N_q. For larger values of N_q the height of the peak also decreases and moves to the lower right in the diagram.

Figure 9B shows p_{KS} as a function of N_q and P_{cut} for $i' = 50°$. Note that P_{cut} and N_q are not well constrained. There is a region with $P_{cut} \lesssim 90$ years and $5000 \lesssim N_q \lesssim 20000$ in which very good models occur.

If we look at all of our models and define a 'reasonable' model as one with $p_{KS} > 0.25$, we find that we cannot constrain P_{cut} at all. There are models with $p_{KS} > 0.25$ for any value of $P_{cut} < 170$ years. However, we find that N_q must be greater than 3000 returns. Models with $N_q \lesssim 3000$ tend to contain HTCs with semi-major axes which are larger than is observed. A large N_q implies that there is very little physical evolution of the comets once they become HTCs. Before they evolve onto HTC orbits, we find that more than 94% of our comets suffer more than 100 returns and 50% suffer more than 500 returns. Thus, we find no significant physical evolution between a few hundred and a few thousand returns. Note that these models do not place any constraints on the physical evolution of comets *before*

they become HTCs, nor on those that do not become HTCs. Our results are consistent with previous estimates of the physical evolution of long-period comets, which find that although most comets fade rapidly, those that survive more than ~ 6 perihelion passages typically remain active for many orbits thereafter (Weissman 1979; 1980; Wiegert & Tremaine 1999). We return to this issue below.

Formally, $20 < i' < 70°$. Indeed, the largest p_{KS} for a model with $i' = 90°$ (an isotropic distribution) is 0.03. Thus, we can conclude with some confidence that an isotropic Oort cloud cannot produce the Halley-type comets that are currently observed. A flattened distribution is required.

In order to test whether inclination biases could affect these conclusions, we generated a series of models similar to those above, but we added an extreme version of this bias. If HTCs were discovered during an observing campaign that only searched near the ecliptic, then the probability that a comet is detected is proportional to the fraction of time it spends near the ecliptic[2]. This probability is proportional to $1/\sin(i)$. However, this is only true for inclinations larger than the height above and below the ecliptic that the search covers. For inclinations smaller than this, the probability is uniform. Thus, we set the probability that a comet is discovered to

$$p_i = \begin{cases} 1 & \text{if } i < 10° \\ \sin(10°)/\sin(i) & \text{if } i \geq 10°, \end{cases} \tag{9}$$

The largest p_{KS} for model with $i' = 90°$ is 0.03. Therefore, we can rule out the isotropic models. The best fit model has $i' = 65°$, which is somewhat larger than the best fit model without the inclination bias, but is consistent with the range of i' derived from the previous models.

The models above seem to indicate that an isotropic Oort cloud cannot be the source of the HTCs and that a flattened distribution with a median inclination similar to that of the observed distribution (45°) is required. We can understand this result by going back to Figure 6. Recall that this figure shows that the inclination of comets is roughly conserved during the capture process. This implies that the inclination distribution of the source region must be roughly similar to the inclination distribution of the HTCs. However, the capture probability must be taken into account in this argument. So to be more precise, the inclination distribution of the Oort cloud multiplied by the probability of capture (as

[2]HTCs were not, in general, discovered in this way; thus the real bias is less severe then that assumed here. Indeed, Everhart (1967) estimated that only roughly 10% of the high inclination LPCs should be lost due to observational biases. HTCs should have similar biases since they were, in general, discovered with similar techniques.

a function of initial orbital elements) must be approximately the same as the inclination distribution of the HTCs. This becomes an issue in the next section.

5. A Two Component Oort Cloud Model

There is another set of observations that we have not yet considered that also must be taken into account. The dynamically new long-period comets are arriving from the Oort cloud and directly measure the inclination distribution of the Oort cloud for $a \gtrsim 20,000\,\mathrm{AU}$. This inclination distribution is nearly isotropic, apparently at odds with our result from above that the source of the HTC must be flattened. One possible solution to this problem is to have an Oort cloud that is isotropic in its outer regions, but is flattened in its inner regions. Such a structure has been suggested previously (DQT87). However, the HTCs may be supplying us with direct evidence for such a structure. Therefore, in this section we expand our model of the Oort cloud to include an inclination distribution that varies as a function of semi-major axis. This model includes the three free parameters in the models above: i', P_{cut}, and N_q. In addition, we add an additional parameter that represents the 2-component structure of the Oort cloud.

We assume that the inner part of the Oort cloud is represented by a flattened population with an inclination distribution given in Equation (7) with i' being a free parameter. The outer part of the Oort cloud is assumed to be isotropic. Since the observed inclination distribution of long-period comets (hereafter LPCs) is isotropic, we assume that the transition between these two regions is at $a = 20,000\,\mathrm{AU}$, which roughly corresponds to the inner edge of the population of the dynamically new long-period comets. We vary the mass ratio between the inner and outer regions. Since we are constructing a Monte Carlo simulation based on the integrations above, we accomplish this by only including a fraction of the particles in the outer region. This fraction, w_{out}, is the additional free parameter for our models. The inverse of w_{out} is an enhancement factor which gives the ratio of the mass of the inner disk in the two-component model to the mass of the inner disk in the one-component model with the same i' (§2).

Therefore, we have 4 free parameters to vary. As with the model in §4, we generate a series of experiments with various values of these parameters and compare the resulting HTC a–i distribution with the observations. The parameters i', P_{cut}, and N_q are sampled the same way as with the one-component models. We chose values of w_{out} between 0.001 and 1 with a spacing in $\log(w_{out})$ of 0.4 (roughly a factor of 2.5). The lower limit of w_{out} is set by a limitation in the integrations: below this value, small number statistics start to dominate our results.

Determining the range of parameters that produce viable models is more difficult than for the one-component models above because many of the two-component models only have a few tens of comets in them. Because of small-number statistics, there can be a large range of different Monte Carlo representations for each set of parameters. We first attempted to combine a number of different Monte Carlo realizations of a given model and then do a K-S test on the combined model. However, when we constructed the models, we found that the same particle could be included more than once, often many times. This caused the K-S probability to be artificially small, so that the valid models were incorrectly rejected. Therefore, we developed the following procedures for determining which models are reasonable.

We first reject any model with $p_{KS} < 0.05$. For each model with larger p_{KS}, we generate an additional 6 Monte Carlo realizations and compute p_{KS} for each of the 6 a–i distributions. Define $\langle p \rangle$ as the average of the 6 p_{KS}'s. In order to calculate the significance level corresponding to $\langle p \rangle$, we perform the following experiment *for each set of parameters.* 1) We generate a realization of the model that contains the same number of comets (22) as the observed HTC population with $q < 1.3\,\mathrm{AU}$. We use this as our control sample. 2) We calculate a parameter $\langle p_c \rangle$ using the above procedures for $\langle p \rangle$ but using our control rather than the real HTCs. Note that the control is generated by the same model as the 6 realizations used to calculate $\langle p_c \rangle$. 3) We repeat steps (1) and (2) 200 times. The resulting 200 $\langle p_c \rangle$'s represent the distribution that we expect if the two distributions were derived from the same parent distribution. Therefore, we define our confidence level, c, as the fraction of the $\langle p_c \rangle$'s that are less than $\langle p \rangle$. Again, we performed this calculation for each of our candidate models.

The model with the largest c is

- $i' = 20°$
- $P_{cut} = 30$ years.
- $N_q = 5000$ passages.
- $w_{out} = 0.001$.
- $c = 0.6$.

Figure 10 shows the cumulative semi-major axis, inclination, and perihelion distance distributions of this model. The semi-major axis and perihelion distance distributions match the observations fairly well. However, the model's inclination distribution is slightly more isotropic than the observed distribution. In particular, the median inclination of this model

is 53°, while the real HTCs have a median inclination of only 45°. The fact that c is large indicates that this discrepancy could be due to small number statistics. Recall that there are only 22 known HTCs in our sample. In addition, perhaps a better agreement could be found if we allowed for smaller values of w_{out} (see below).

If we define a reasonable model as one with $c > 0.1$, then we can constrain the values of our free parameters to:

- $10° \leq i' \leq 50°$
- P_{cut} is not constrained.
- $N_q \geq 5000$ passages.
- $0.001 \leq w_{out} \leq 0.16$.

Figure 11 shows a contour plot of a 'projection' of the c distribution in i'–w_{out} space, which are the two parameters that represent the structure of the Oort cloud. By 'projection' we mean that for each value of i' and w_{out}, we took the maximum value of c along the other parameters. There is a peak centered on our best fit model at $i' = 20°$ and $w_{out} = 0.001$, with a shallow falloff away from the peak. The best fit models have $15° \lesssim i' \lesssim 30°$, although i' can be as large as $\sim 50°$.

Although from Figure 11 we find that w_{out} can be as large as 0.15, the best fit models have $w_{out} \lesssim 0.001$. This result indicates a fairly massive inner Oort cloud relative to the outer cloud. Indeed, the fact that the peak of the distribution lies at the lower limit of the figure suggests that we would achieve better fits if we could use smaller values of w_{out}. The need for a massive inner Oort cloud can be understood using the following argument.

The primary result of the models presented in §4 was to show that the inclination distribution of objects entering the planetary region from the Oort cloud must be similar to the inclination distribution of the HTCs. Recall that in our initial model of the Oort cloud, we included the effects of the Jupiter barrier by truncating the inner edge of the initial perihelion distribution at different locations depending on the semi-major axis (see Eq. 1). Particles from the inner regions of the Oort cloud therefore all had large initial perihelion distances. Figure 5B shows the averaged binned probability as a function of perihelion distance. Objects with large perihelion distances are much less likely to get captured than objects with small perihelion distances. Thus, in our model, objects from the inner cloud are less likely to be captured than objects from the outer cloud. It then follows that the inner cloud must be massive in order to supply enough comets to reproduce the HTCs' inclinations.

Unfortunately, it is difficult to interpret the exact meaning of w_{out}. It is not trivial to estimate the mass of the inner cloud because it is dependent on the rate at which Oort cloud comets evolve onto orbits that enter the planetary region. This, in turn, is dependent on the exact semi-major axis and perihelion distance distributions in the cloud. Perhaps a more fruitful approach is to estimate the expected number of long-period comets from our models because that requires us to make the fewest assumptions. We can then compare this prediction to observations.

There are 22 observed HTCs with $q < 1.3\,\mathrm{AU}$. However, this is an underestimate due to observational selection effects. We can correct for the effects of P_{cut} in this distribution by scaling each comet with an orbital period greater than P_{cut} by P/P_{cut}. We call the resulting estimate $N_{HTC,q}$, which is 57 for our best fit model above ($P_{cut} = 30$ years). Note that this represents active comets only.

We can use our model to estimate the average lifetime of a HTC, L_{HTC}. To be more precise, L_{HTC} is the average length of time that a comet is an active HTC with $q < 1.3\,\mathrm{AU}$. For our best fit model $L_{HTC} = 75,000$ years. This number takes into account the dynamical evolution of HTCs as well as their physical evolution (through N_q). The rate at which new HTCs are created in this model is $R_{HTC} = N_{HTC,q}/L_{HTC}$, which is 7.6×10^{-4} comets per year.

We can also use our model to estimate the probability that once an Oort cloud comet enters the planetary system from the Oort cloud, it will become an HTC with $q < 1.3\,\mathrm{AU}$. For our best fit model, $p = 1.6 \times 10^{-4}$. The rate at which Oort cloud comets must be entering the planetary system is therefore $R_{Oort} = R_{HTC}/p$, which is 4.9 comets per year in our best fit model.

The above estimate is for all comets from the Oort cloud entering the planetary system, independent of the comet's perihelion distance. However, we have built into our models a perihelion distribution for objects first entering the planetary system (see §2 and in particular Figure 3). The distribution will be somewhat modified by our choice of w_{out}. In our best fit model, the fraction of new comets entering the planetary system with $q < 1\,\mathrm{AU}$, f_q, is 1.4×10^{-3}.

Therefore, we can predict the expected rate of LPCs with $q < 1\,\mathrm{AU}$ to be $R_{LPC} = R_{Oort}\, f_q$, which is ~ 0.006 dynamically new comets per year in our best fit model. Indeed, applying this argument to all models with $c > 0.1$, we find that $0.0012 < R_{LPC} < 0.015$. Wiegert & Tremaine (1999) argue that in the Solar System there are roughly 12 dynamically new comets per year with $q < 3\,\mathrm{AU}$, which implies ~ 4 per year with $q < 1\,\mathrm{AU}$ (also see Weissman 1985). There is a discrepancy of over two orders of magnitude between our model

predictions and the observations! This is consistent with a previous study of the HTCs by Emel'yanenko & Bailey (1998).

There are large uncertainties in the above estimates of R_{LPC} due to the assumptions in our models. Our most severe assumption is our adopted initial perihelion distribution for the comets, see §2 and Figure 2. In order to test the sensitivity of our results to this assumption, we constructed a model that has the same i', N_q, and P_{cut} as our best fit model, but a different initial perihelion distribution. We chose $q_i = 6\,\mathrm{AU}$ and set $\rho_\circ = 0.22\,M_\odot/pc^3$ so that $(q_i - \Delta q) = 1\,\mathrm{AU}$ for $a = 20,000\,\mathrm{AU}$. Since the fraction of the model's particles initially beyond $20,000\,\mathrm{AU}$ is a function of both w_{out} and the initial q distribution, we adjusted w_{out} to 0.002 so that this fraction was preserved. For this model $R_{LPC} = 0.009$, similar to the value for our best fit model. So, changing our initial perihelion distance distribution will not solve the inconsistency between our model and the observed LPCs. Indeed, we have found that it is not possible to solve this inconsistency by adjusting any of our parameters, even to extreme values.

Is it possible to reconcile our models with this low predicted rate of long-period comets? Another way to view this problem is that given the observed rate of LPCs, we would expect to see about two orders of magnitude more HTCs than are actually observed. One possibility is that over 99% of the comets from the Oort cloud become extinct or disintegrate before they can become HTCs. Figure 12 shows the cumulative distribution of the number of perihelion passages less than 2.5 AU that a comet has suffered in our best fit model. If we are to argue that only 1 comet in 100 remains active until it becomes a HTC, then from the figure this fading must occur before a comet suffers 230 perihelion passages (1% of comets in the model have suffered fewer than 230 perihelion passages). In fact, the die-off must have occurred much earlier than that if we require that it not affect the observed HTC distribution. Given this argument and the large N_q of our models (which suggests very little physical evolution of comets as HTCs), the most plausible conclusion is that most comets fade or disintegrate during their first few passages and the remainder are unchanged for long periods of time.

Indeed, there is observational evidence for such fading in the orbits of the LPCs themselves. Over the years, many researchers have modeled the dynamical behavior of dynamically new long-period comets as they evolve (Oort 1950; Whipple 1962; Weissman 1980; Wiegert & Tremaine 1999)[3]. They have always found that the ratio of the number of 'returning' comets to the number of dynamically new comets in their models is significantly larger than observed. Despite valiant efforts to explain this discrepancy with dynamics alone,

[3]To be more precise, the efforts have concentrated on what Levison (1996) calls 'external' comets. Halley-type comets are usually not considered.

it was found that the only way to change the models so that they match the observations is to allow the comets in the models to physically age. That is, comets must fade and become extinct (or disintegrate) as a function of time. The most recent attempt at this (Wiegert & Tremaine 1999) found a good match if: (1) the fraction of comets remaining visible after m apparitions is proportional to m^{β} where $\beta = -0.6 \pm 0.1$, or (2) if $\sim 95\%$ of comets live for only ~ 6 returns and the remainder last indefinitely (also see Weissman 1980).

Our models of the HTCs are consistent with these ideas. Perhaps, however, we need a somewhat steeper fading law. For example (1) predicts that 4% of the comets should remain after 230 apparitions, while we require less than 1%. If we assume that we require 1% after 200 apparitions, we find that $\beta \sim -0.8$. This number is very uncertain, since it most likely depends on the exact semi-major axis and perihelion distance distributions of the Oort cloud.

Another interesting question is whether objects from the Oort cloud (particularly the inner Oort cloud) can be contributing to the Jupiter-family comet (JFC) population (those comets with Tisserand parameters between 2 and 3, see Levison [1996]). These objects typically have orbit periods less than 20 years and very small inclinations. We can estimate from our models the fraction of active comets with $q < 1.3\,\mathrm{AU}$ and $a < 34\,\mathrm{AU}$ that are JFCs, f_{JFC}. Since our models have observational biases built into them in the form of P_{cut}, we can directly calculate the expected number of active Oort cloud JFCs from the observed number of HTCs. We find that $0.04 < f_{JFC} < 0.23$ for models with $c > 0.1$, with a median value of 0.1. Our best fit model has $f_{JFC} = 0.15$.

As discussed above, there are 22 known HTCs with $q < 1.3\,\mathrm{AU}$, which implies that we may expect that between 1 and 5 active JFCs with $q < 1.3\,\mathrm{AU}$ originated in the Oort cloud. The median value is 2 comets and our best fit model predicts 4 JFCs. There currently are 32 known active JFCs with $q < 1.3\,\mathrm{AU}$. So, although we do not expect Oort cloud comets to dominate the JFC population, several of the known JFCs may have originated in the Oort cloud. However, the orbital elements of the JFCs produced in our models are usually different from those of the observed JFCs. For example, the median Tisserand parameter, T, of the observed JFCs is 2.8, while only 5% of the JFCs produced in models with $c > 0.1$ have $T > 2.8$. Thus, if the Oort cloud does contribute to the JFCs, it mainly contributes to the outliers of the population.

Along similar lines is the issue of whether objects from the Oort cloud can be contributing to the Centaur population. Centaurs are usually large (diameters larger than ~ 50km), inactive objects found in the outer solar system. As such, activity is not a requirement for their discovery as it is for the JFCs and HTCs. In addition, Centaurs do not suffer from the same observational biases as the comets and thus we will ignore P_{cut} in the following

estimate. Therefore, we will be estimating the total number of Centaurs that originated in the Oort cloud as opposed to the number that we have observed. Also, we are assuming that the 'fading' described above is due to objects becoming extinct rather than disintegrating and thus there is no loss as objects become Centaurs. Again, we will use our best fit model.

As discussed above, we estimate that $N_{HTC,q} = 57$ for our best fit model. This number refers to active comets only. We can crudely estimate the fraction of comets that are active by taking the ratio R_{LPC} from our models to that derived from the observations, which is (see above) $0.006/4 = 0.0015 \equiv r_{act}$ for our best fit model. We also estimate in our models the fraction of objects with $a < 34\,\mathrm{AU}$ that have $q < 1.3\,\mathrm{AU}$, r_q. For our best fit model $r_q = 0.0022$. Thus, our best fit model contains $N_{HTC} = N_{HTC,q}/(r_{act} r_q) = 1.7 \times 10^7$ objects with $a < 34\,\mathrm{AU}$. Applying this argument to all our models with $c > 0.1$, we find that $10^6 < N_{HTC} < 2 \times 10^8$. This can be compared to an estimate of roughly 10^6 objects in the same region of the solar system from the Kuiper belt (Levison & Duncan 1997; call this value N_{KB}). These values of N_{HTC} refer to objects with diameters larger than roughly 1km.

Is it reasonable to suppose that the Oort cloud is supplying a significant fraction of the Centaurs? A defining characteristic of the Centaurs is their inclination distribution. The average $\cos(i)$ of 13 multiple opposition Centaurs with $a < 34\,\mathrm{AU}$ is 0.97, which corresponds to an inclination of $\sim 14°$. Furthermore they all have inclinations less than 25°. The average $\cos(i)$ if the same population as predicted by our best fit model is 0.84, which corresponds to $i = 33°$. Although we believe that this difference is significant, a direct comparison is difficult because of the observational bias in the observed distribution. Although the inclination bias is not significant for the HTCs (Everhart 1968), it is significant for the Centaurs because many were discovered during searches for Kuiper belt objects, which suffer from these biases (Jewitt et al. 1996).

Another comparison can be made with the eccentricities of these objects. In order to remove the most important observational bias, that with respect to perihelion distance, we will only consider those objects with $5\,\mathrm{AU} < q < 10\,\mathrm{AU}$ and $a < 30\,\mathrm{AU}$. The observed multiple opposition Centaurs that meet these criteria have a mean eccentricity of 0.47 ± 0.03. The models of Levison & Duncan (1997) predict $\overline{e} = 0.50$ for this subset of the Centaurs. For our best fit model, $\overline{e} = 0.61$. So both from the inclination and eccentricity distributions it is unlikely that the Oort cloud is the dominant source of the Centaurs.

So, how do we reconcile the inclination distribution with our conclusion that by numbers the Oort cloud should be the dominant source of the Centaurs? There are several reasons why our estimate for N_{HTC} could either be too large or not relevant to the larger Centaurs. *i*) The value of N_{HTC} is very sensitive to the assumed fraction of new comets entering the planetary system with $q < 1\,\mathrm{AU}$, f_q, which is an input into our models (see Equation 1

and Figure 2). For example for our best fit model, $f_q = 1.4 \times 10^{-3}$. The assumption that would maximize f_q would be to take a uniform perihelion distance distribution. In this case $f_q = 3 \times 10^{-2}$ and N_{HTC} decreases by a factor of 20. *ii*) The above comparison between N_{HTC} and N_{KB} is for comet-size objects not the larger Centaurs. If objects originating in the Oort cloud had a much steeper size distribution than Kuiper belt objects then it is possible that the Kuiper belt could be the dominant source of the observed Centaurs. *iii*) In calculating N_{HTC} we assume that when objects fade they become extinct and do not disintegrate. If these objects disintegrated, they would not become Centaurs. However, although disintegration seems a reasonable mechanism for small comet-sized objects, it does not seem as likely for objects as large as the observed Centaurs. Clearly the issue of Centaurs is an important one for the viability of the models presented here. We will investigate them more in a future manuscript.

One possible solution to the above difficulties is to decouple the current flux of LPCs from the current number of HTCs and Centaurs. This could happen during a comet shower (Hills 1981; Heisler & Tremaine 1986; Heisler 1990). For example, one could imagine that at the beginning of the shower, the influx of LPCs is increased before the number of HTCs and Centaurs could be affected. If we lived during such a period, we would see an enhanced LPC flux compared to the HTC population, which is consistent with observations. However, there is a major problem with such an idea. At early times of a shower the LPC population will not be isotropic. Indeed, it takes roughly 3–5 million years for the LPC population to become isotropic after the start of a shower (Heisler et al. 1991; Weissman 2000; pers. comm.). On the other hand, the median age (time since a comet first penetrated the planetary system) of the HTCs in our best fit model is also 3 million years. Thus, it is unlikely to see both an enhancement in the LPC flux compared to the HTC population *and* an isotropic LPC population as observed today. We will investigate the role of a time varying flux in future works.

We now return to some dynamical considerations. Objects in the inner Oort cloud have initial perihelion distances beyond Saturn and initial semi-major axes which imply that galactic tides alone cannot bring them into the inner Solar System. It is thus interesting to investigate the dynamical pathways these comets follow to become HTCs. We find that there are three distinct dynamical mechanisms that can be responsible for this evolution, which are illustrated in Figure 13. Roughly 70% of the objects from a flattened inner Oort cloud that evolve to small-perihelion HTCs are brought into the planetary region due to the effects of the giant planets (primarily Uranus and Neptune). Figure 13A shows a typical trajectory. The object initially is on an orbit with a perihelion distance near the orbit of Uranus. Gravitational encounters with Uranus cause a random walk in semi-major axis. In this case the object's a decreases while q remains constant until it reenters the planetary

system. After a drops below $\sim 30\,AU$, Uranus hands the object off to Saturn, which in turn hands it to Jupiter. Jupiter then scatters the object into the inner Solar System.

Figure 13B shows another possible trajectory. This particle initially has a perihelion distance beyond Saturn. However, at 8×10^5 years, a passing star of $0.5\,M_\oplus$ and an impact parameter $74,000\,AU$ lowers its perihelion to inside Jupiter's orbit. Note that the particle's semi-major axis is constant during the encounter. Jupiter then scatters the object into the inner Solar System. So, although on average galactic tides dominate the evolution of q of Oort cloud comets, for some objects rare passing star events can be the most important perturber.

The last important dynamical process is illustrated in Figure 13C. The object has an initial perihelion distance of $\sim 20\,AU$. Repeated encounters with Uranus cause a random walk in semi-major axis. At about 4 Myr the semi-major axis is kicked to above $15,000\,AU$ where galactic tides become important. As a result, the perihelion distance starts to slowly decrease. This is accelerated when the semi-major axis increases to $20,000\,AU$. The object evolves onto a Saturn-crossing orbit due to the tides, after which the object is drawn into the planetary system and evolves into a small-perihelion HTC.

Finally, these three processes can combine in order to produce HTCs. The object shown in Figure 13D is a typical example. Here the object had an initial perihelion distance near Uranus' orbit. The same passing star responsible for the behavior seen in Figure 13B lowers this particle's perihelion to just inside Saturn's orbit. The particle encounters Saturn, causing a random walk in semi-major axis. During this time the semi-major axis gets as small as $2700\,AU$. At roughly 2 Myr, the semi-major axis becomes $29,000\,AU$, after which galactic tides become important and q evolves inward, until at ~ 6 Myr it is at $\sim 2.5\,AU$. A stellar encounter then lowers its perihelion distance to $\sim 0.8\,AU$. Note that the object's semi-major axis is still $29,000\,AU$, so the particle is now considered a dynamically new long-period comet. Multiple encounters with the planets then draw the comets into an HTC orbit.

The behavior illustrated in Figures 13C and 13D raises an intriguing possibility — a significant fraction of the dynamically new long-period comets could originate in a flattened inner Oort cloud. In this scenario, the perihelia of objects originally with semi-major axes significantly less than $20,000\,\mathrm{AU}$ and with modest inclinations evolve into the realm of the giant planets. Gravitational interactions with the giant planets raise the semi-major axes of these objects beyond $20,000\,\mathrm{AU}$, where galactic tides or passing stars can inject them into visible ($q \lesssim 2.5\,\mathrm{AU}$) orbits in one orbital period. We believe that this may be an important process. However, the difficulties associated with the fading problem described above make it extremely difficult to quantify its importance.

6. Conclusions

Previous models (e.g., DQT88) of the formation of HTCs have failed to reproduce the observed inclination distribution, which has a median inclination of only 45°. These models have assumed an isotropic Oort cloud. This discrepancy raises the intriguing possibility that the study of the HTCs may allow us to probe the structure of the Oort cloud — particularly the inner Oort cloud which does not directly produce visible comets.

We have integrated the orbits of 27,700 test particles initially entering the planetary system from the Oort cloud, under the gravitational influence of the Sun, giant planets, passing stars, and galactic tides. The particles were initially distributed roughly uniformly in semi-major axis and cosine of the inclination. The perihelion distribution is constructed to account for the so-called 'Jupiter Barrier' (see §2 for details). The orbit of each particle was integrated for up to 1 billion years or until it was either ejected from the system, hit the Sun or a planet, or evolved onto an orbit that no longer entered the planetary region. We found that the resulting HTC population is inconsistent with the observed distribution.

We have adjusted our assumed structure for the Oort cloud by selecting particles in our simulations based on their initial orbits. In addition, we have included the effects of physical aging and observational biases by removing particles based on their osculating orbital elements. We found that in order to match the a–i distribution of the HTCs, the initial Oort-cloud inclination distribution of the comets that become HTCs must have a median inclination, i', less than 70°, with the value most likely near 50°. This is because we find that, on average, the inclination of comets is roughly conserved during the capture process. Thus, the inclination of the HTC comets when they were in the Oort cloud must be similar to the observed population.

We constructed 2-component models of the Oort cloud with an isotropic outer cloud and a disky inner cloud. The transition region was set to 20,000 AU. Our best fit model had $i' = 20°$ for the inner disk. We found, however, that $i' \lesssim 50°$. All these models required an inner Oort cloud that was significantly more massive than a cloud with a distribution that is uniform in a. This is due to the fact that objects from the inner cloud were less likely to be captured than objects from the outer cloud. So we must have a massive inner cloud to supply enough comets to produce an inclination distribution similar to what is seen. This model also predicts that some of the Jupiter-family comets could have originated in the Oort cloud.

Our models predict too few observed HTCs compared to the observed number of dynamically new long-period comets. This inconsistency is most likely related to the well-known 'fading problem' for long-period comets (Oort 1950; Whipple 1962; Weissman 1980;

Emel'yanenko & Bailey 1998; Wiegert & Tremaine 1999). Our models appear to require a steeper fading law than has been previously suggested. These models also appear to be producing a Centaur population that is inconsistent (in numbers and orbital elements) with the observed population. We will investigate this in future works.

We would like to thank P. Weissman and the Nice dynamics group for useful discussions. We are also grateful to T. Quinn for acting as the referee for this paper. His comments led to significant improvements in the text. HFL and LD are grateful to NASA's PGG and Origins programs for support. MJD is grateful for the continuing financial support of the Natural Science and Engineering Research Council of Canada.

REFERENCES

Bahcall, J.N. 1984. *Astrophys. J.* **276**, 169.

Bowell, E., West, R.M., Heyer, H.-H., Quebatte, J., Cunningham, L.E., Bus, S.J., Harris, A.W., Millis, R.L., & Marsden, B. G. 1992. *IAU Circ.*, **5585**, 1.

Carusi, A., Kresák, L. & Valsecchi, G. 1987. A&A, **187**, 899.

Creze, M., Chereul, E., Bienayme, O., & Pichon, C. 1998. *Astron. Astrophys.*, **329**, 920.

Duncan, M., & Levison, H. 1997. *Science*, **276**, 1670.

Duncan, M., Quinn, T., & Tremaine, S. 1987. *Astron. J.* **94**, 1330.

Duncan, M., Quinn, T., & Tremaine, S. 1988. *Astrophy. J. Lett.*, **328**, L69.

Emel'yanenko, V.V., & Bailey, M.E.: 1998, *Mon. Not. R. Astron. Soc.*, **298**, 212.

Everhart, E. 1967. *Astron. J.*, **72**, 716.

Feast, M., & Whitelock, P. 1997. *Mon. Not. R. Astron. Soc.*, **291**, 683.

Fernández, J.A. 1997. *Icarus*, **129**, 106.

Gaidos, E.J. 1995. *Icarus* **114**, 258.

Heisler, J., & Tremaine, S. 1986. *Icarus* **65**, 13.

Heisler, J., Tremaine, S., Weissman, P., & Greenberg R. 1991. *LPSC* **XXII**, 553.

Heisler, J. 1990. *Icarus*, **88**, 104.

Hills, J.G. 1981. *Astron. J.*, **86**, 1730.

Holmberg, J., & Flynn, C. 2000. *Mon. Not. R. Astron. Soc.*, **313**, 209.

Jewitt, D., Luu, J., & Chen, J. 1996. *Astron. J.*, **112**, 1225.

Levison, H. 1996. In 'Completing the Inventory of the Solar System', eds. T.W. Rettig & J.M. Hahn. (San Francisco: ASP), 173.

Levison, H.F., & Duncan, M.J. 1994. *Icarus* **108**, 18.

Levison, H.F., & Duncan, M.J. 1997. *Icarus* **127**, 13.

Matese, J., & Whitmire, D. 1996.*Astrophys. J. Lett.* **472**, L41.

Olling, R.P., & Merrifield, M.R. 1998. *Mon. Not. R. Astron. Soc.* **297**, 943.

Oort, J.H. 1950. *Bull. Astron. Inst. Neth.*, **11**, 91.

Pham, H.A. 1997. In *Proceedings of the Hipparcos Venice 97 Conference* (ESA SP 402), B. Battrick, Ed.

Press, W.H., Teukolsky, S.A., Vetterling, W.T., & Flannery B.P. 1992. *Numerical Recipes in FORTRAN*, 2nd Ed. Cambridge Univ. Press.

Quinn, T.R., Tremaine, S., & Duncan, M.J 1990. *Astrophys. J.*, **355**, 667.

Stagg, C.R., & Bailey, M.E. 1989. *Mon. Not. R. Astron. Soc.*, **241**, 507.

Weissman, P. R. 1979. In 'Dynamics of the Solar System', ed. R.L. Duncombe. (Dordrecht: Reidel) 277.

Weissman, P.R. 1980. *Astron. & Astrophy*, **85**, 191.

Weissman, P.R. 1985. In 'Dynamics of Comets', eds. A. Carusi and G.B. Valsecchi (Dordrecht: Reidel) 87.

Whipple, F.L. 1962. *Astron. J.*, **67**, 1.

Wiegert, P. 1996. Unpublished Ph.D. thesis, University of Toronto.

Wiegert, P. & Tremaine, S. 1999, *Icarus*, **137**, 84.

Wisdom, J., & Holman, M. 1991, *Astron. J.*, **102**, 1528.

Fig. 1.— A comparison between the cumulative orbital element distributions of the observed HTCs (dotted curve) and those produced in the models of QTD90 (solid curve). A) The semi-major axis distributions. B) The inclination distributions.

Fig. 2.— Our initial perihelion distance distribution is uniform with a minimum set by the 'Jupiter Barrier' (see text for a description). This figure plots this minimum perihelion distance, which we define as $10\,\mathrm{AU} - \Delta q$. Δq is a function of semi-major axis and is defined in Equation 1.

Fig. 3.— A comparison between the cumulative perihelion distance (q) distributions of the observed HTCs (dotted curve) and those produced in our raw integrations (solid curve). We conclude from this that the discovery probability is independent of q for $q < 1.3\,\mathrm{AU}$.

Fig. 4.— A comparison between the cumulative orbital element distributions of the observed HTCs (dotted curve) and those produced in our raw integrations (solid curve). A) The semi-major axis distributions. B) The inclination distributions. Note the significant disagreement in the inclination distributions.

Fig. 5.— The averaged binned probability that an object is captured into an HTC orbit as a function of its initial orbital elements in the Oort cloud. The errorbars are assuming Poisson statistics. A) Initial inclination. Note the slight enhancements at low inclinations and near 120°. B) Initial perihelion distance. There is a significant enhancement at small perihelion distances.

Fig. 6.— The averaged binned cosine of the inclination of particles in our integration when they are on HTC orbits as a function of their initial inclination in the Oort cloud. We divide our particles into two groups. One group has initial semi-major axes (a) less than $20,000\,\mathrm{AU}$ (filled circles) and the other has $a > 20,000\,\mathrm{AU}$ (open circles). The 'error bars' show the magnitude of the standard deviation in each bin.

Fig. 7.— Our assumed initial cumulative inclination distribution for flattened parts of the Oort cloud. The four curves show this distribution for different values of the median inclination, i'.

Fig. 8.— Same as Figure 4 but for our best fit one component model. This model has $i' = 50°$, $P_{cut} = 50$ years, and $N_q = 8000$. Note that the model is a good representation of the data.

Fig. 9.— Contours of p_{KS} for our one component models. These models have three free parameters: i', P_{cut}, and N_q. Two slices through this three dimensional space are shown. A) $N_q = 8000$ B) $i' = 50°$.

Fig. 10.— A comparison between the cumulative orbital element distributions of the observed HTCs (dotted curve) and those produced in our best fit two component model (solid curve). This model has $i' = 20°$, $P_{cut} = 30$ years, $N_q = 5000$, and $w_{out} = 0.001$. A) The semi-major axis distributions. B) The inclination distributions. C) The perihelion distance distributions. Note that the model is a good representation of the data.

Fig. 11.— Contours of c for our two component models projected along the two axes P_{cut} and N_q. By projected we mean that for each value of w_{out} and i', we plot the maximum value of c.

Fig. 12.— The cumulative distribution of the number of perihelion passages less than 2.5 AU that a comet has suffered in our best fit two component model. A particle is represented in this distribution with its instantaneous value whenever it is an HTC.

Fig. 13.— The temporal behavior of 4 particles from our simulation that become HTCs. The solid curves show the semi-major axes while the dotted curves show the perihelion distances. See text for details.

Figure 1A —

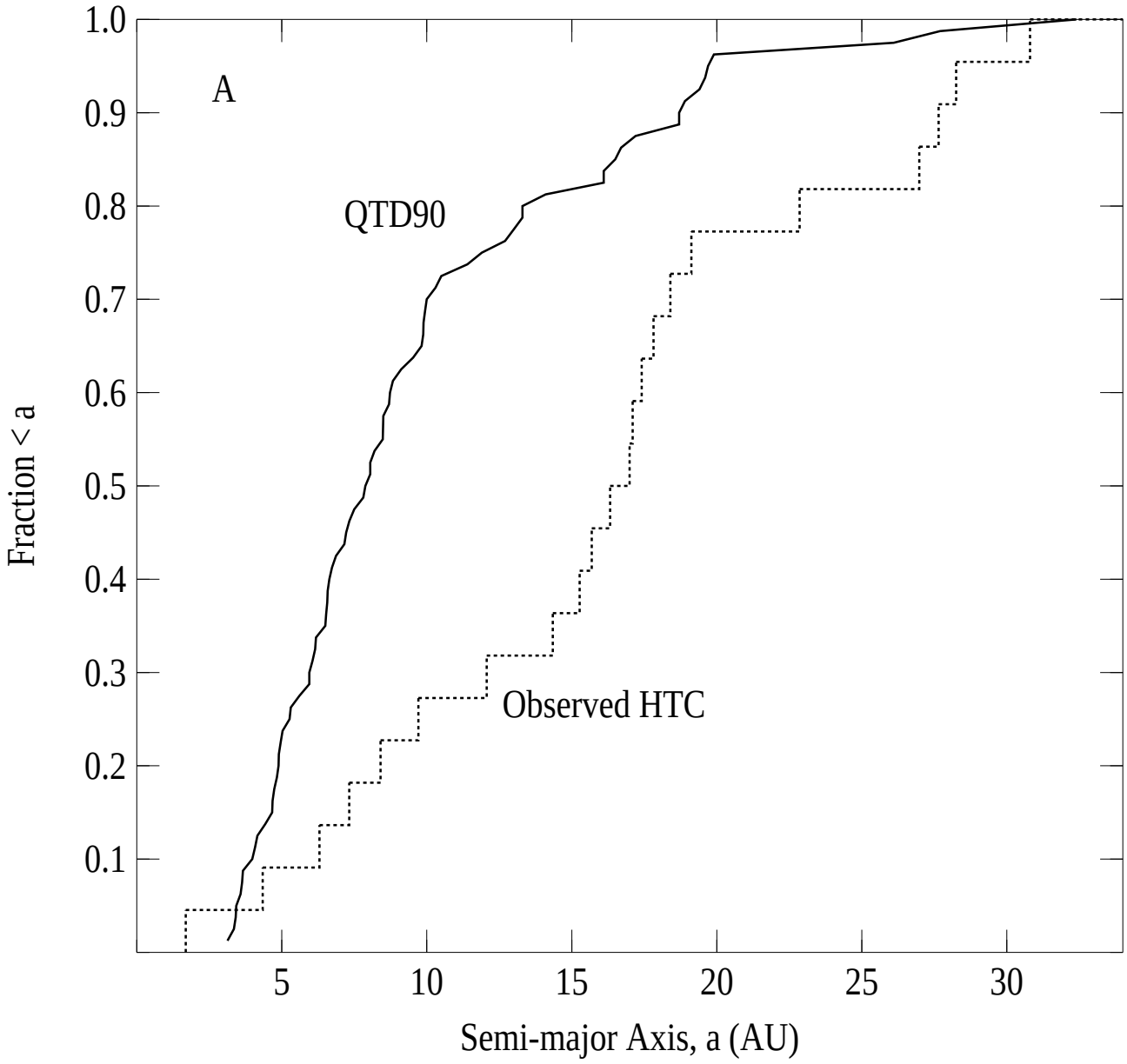
A
QTD90
Observed HTC
Fraction < a
Semi-major Axis, a (AU)
1.0
0.9
0.8
0.7
0.6
0.5
0.4
0.3
0.2
0.1
5
10
15
20
25
30

Figure 1B —

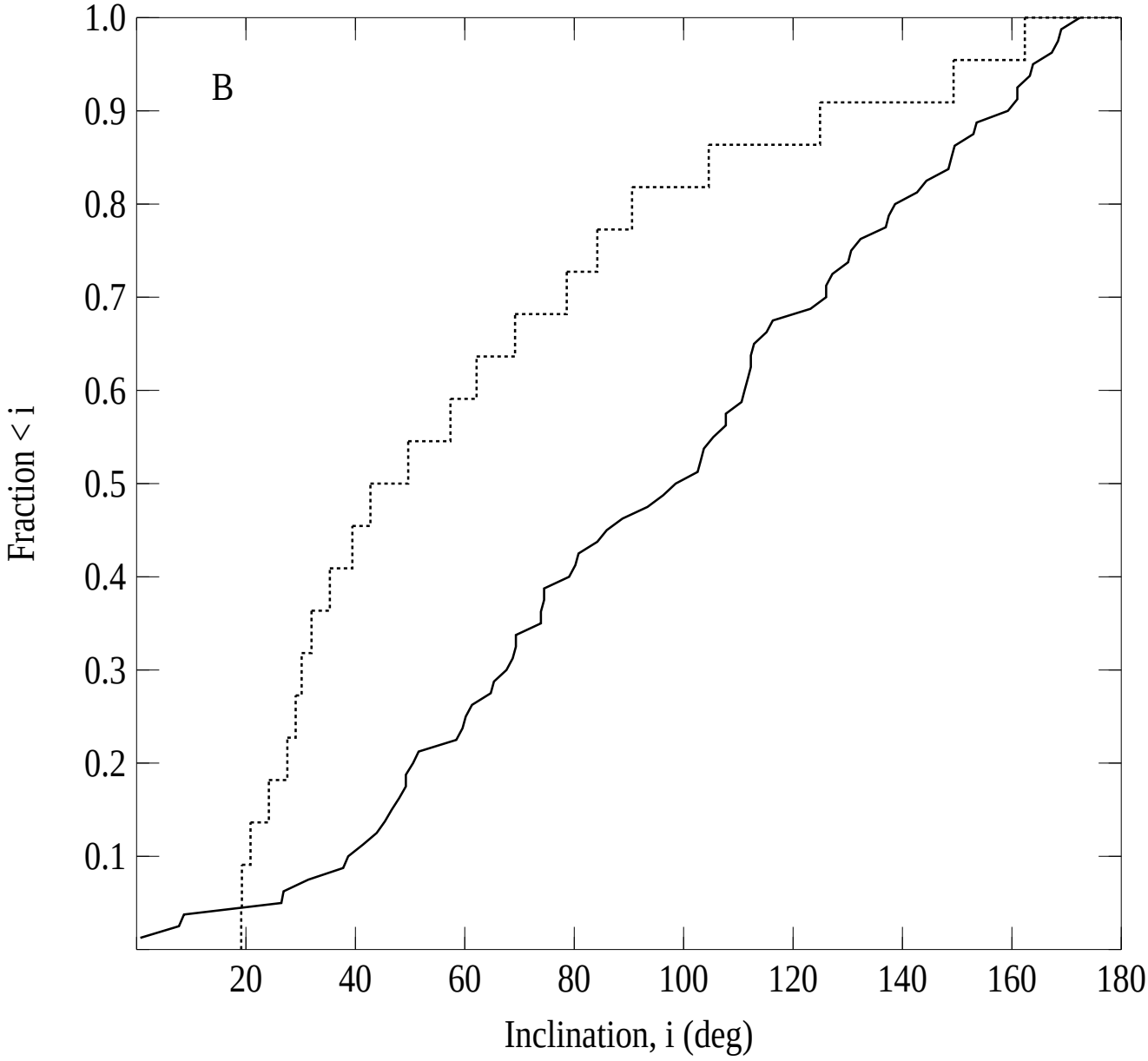
B
Fraction < i
Inclination, i (deg)
1.0
0.9
0.8
0.7
0.6
0.5
0.4
0.3
0.2
0.1
20
40
60
80
100
120
140
160
180

Figure 2 —

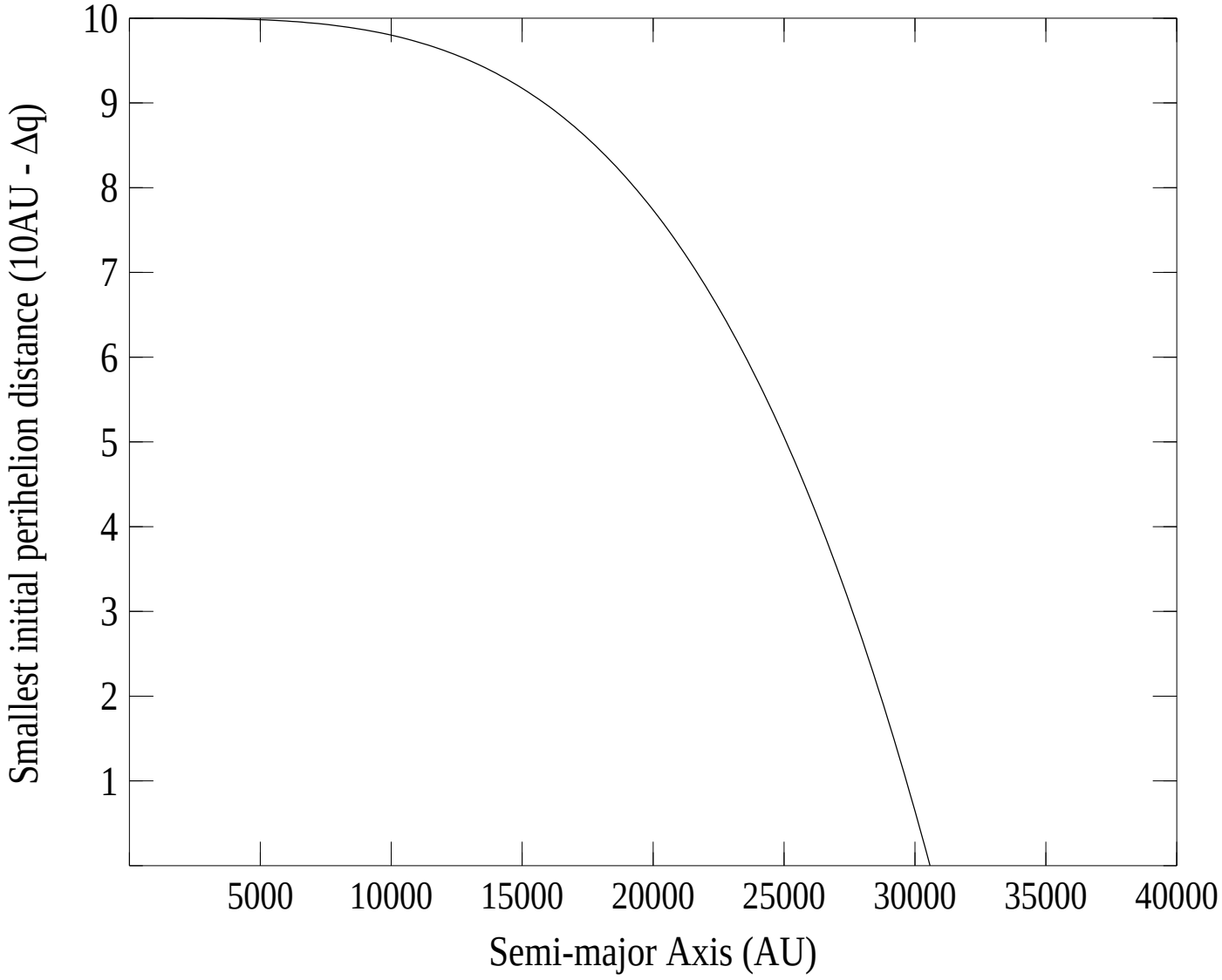
Smallest initial perihelion distance (10AU - Δq)
10
9
8
7
6
5
4
3
2
1
5000
10000
15000
20000
25000
30000
35000
40000
Semi-major Axis (AU)

Figure 3 —

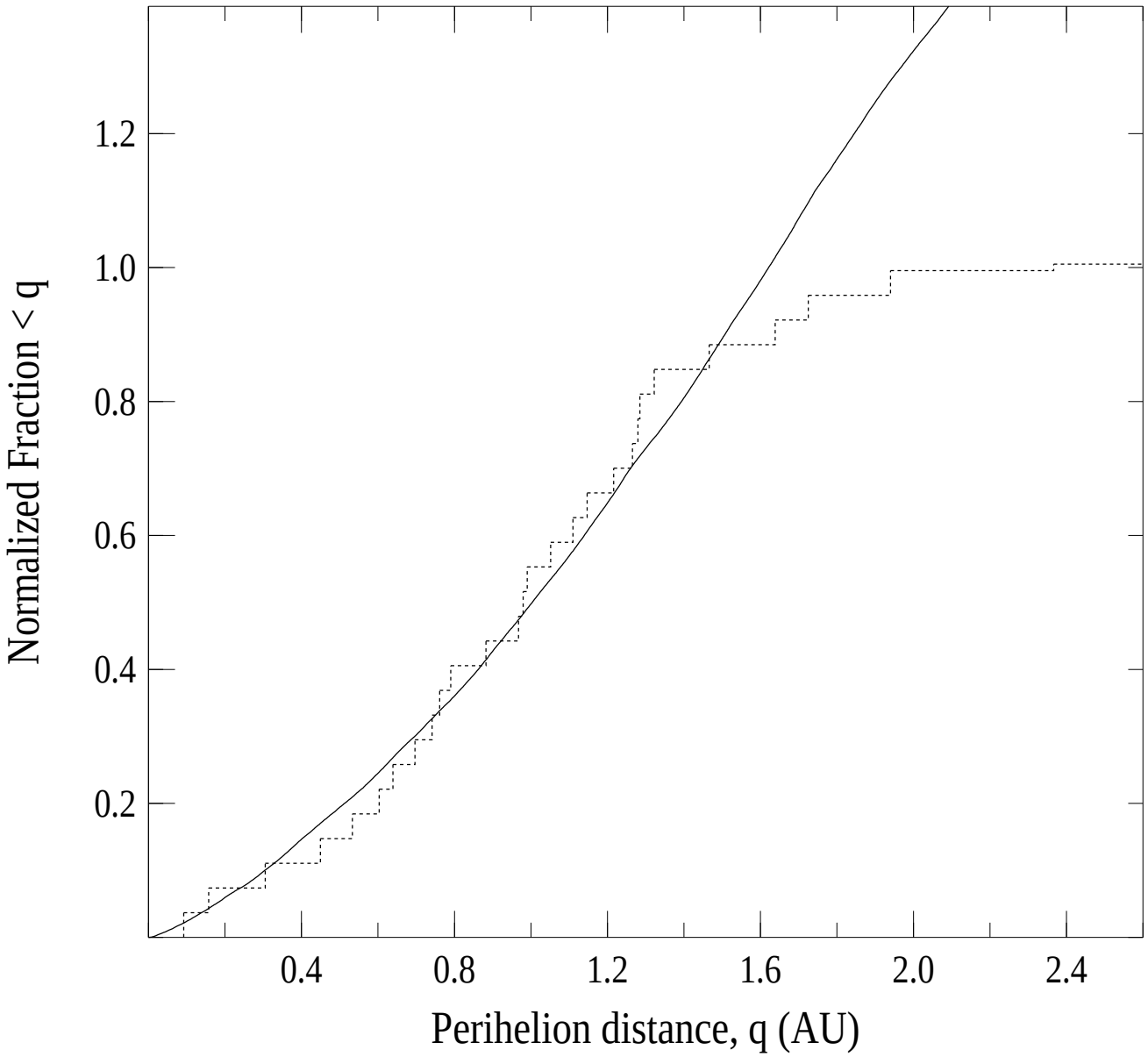
Normalized Fraction < q
1.2
1.0
0.8
0.6
0.4
0.2
0.4
0.8
1.2
1.6
2.0
2.4
Perihelion distance, q (AU)

Figure 4A —

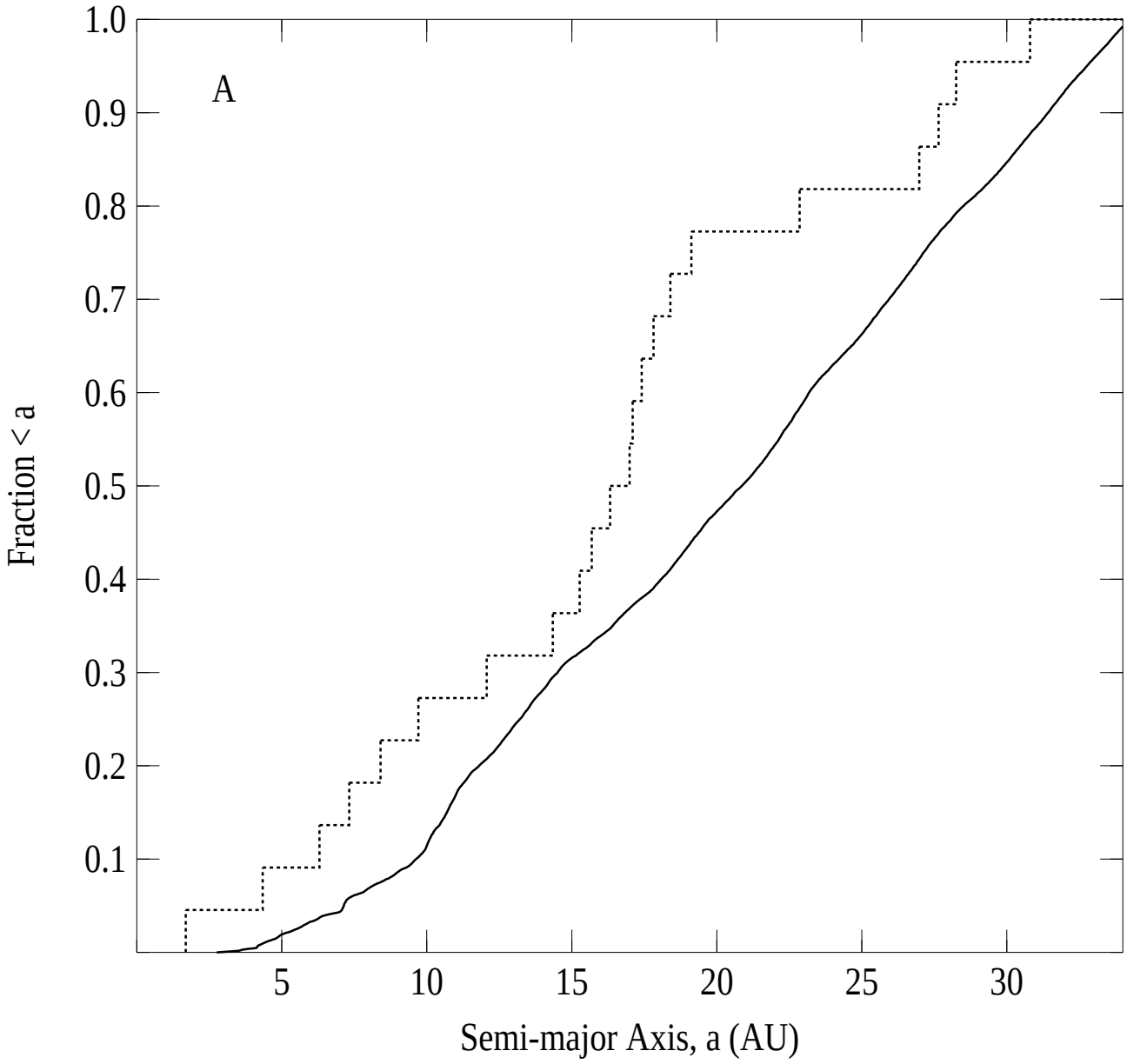
A
1.0
0.9
0.8
0.7
0.6
0.5
0.4
0.3
0.2
0.1
Fraction < a
5
10
15
20
25
30
Semi-major Axis, a (AU)

Figure 4B —

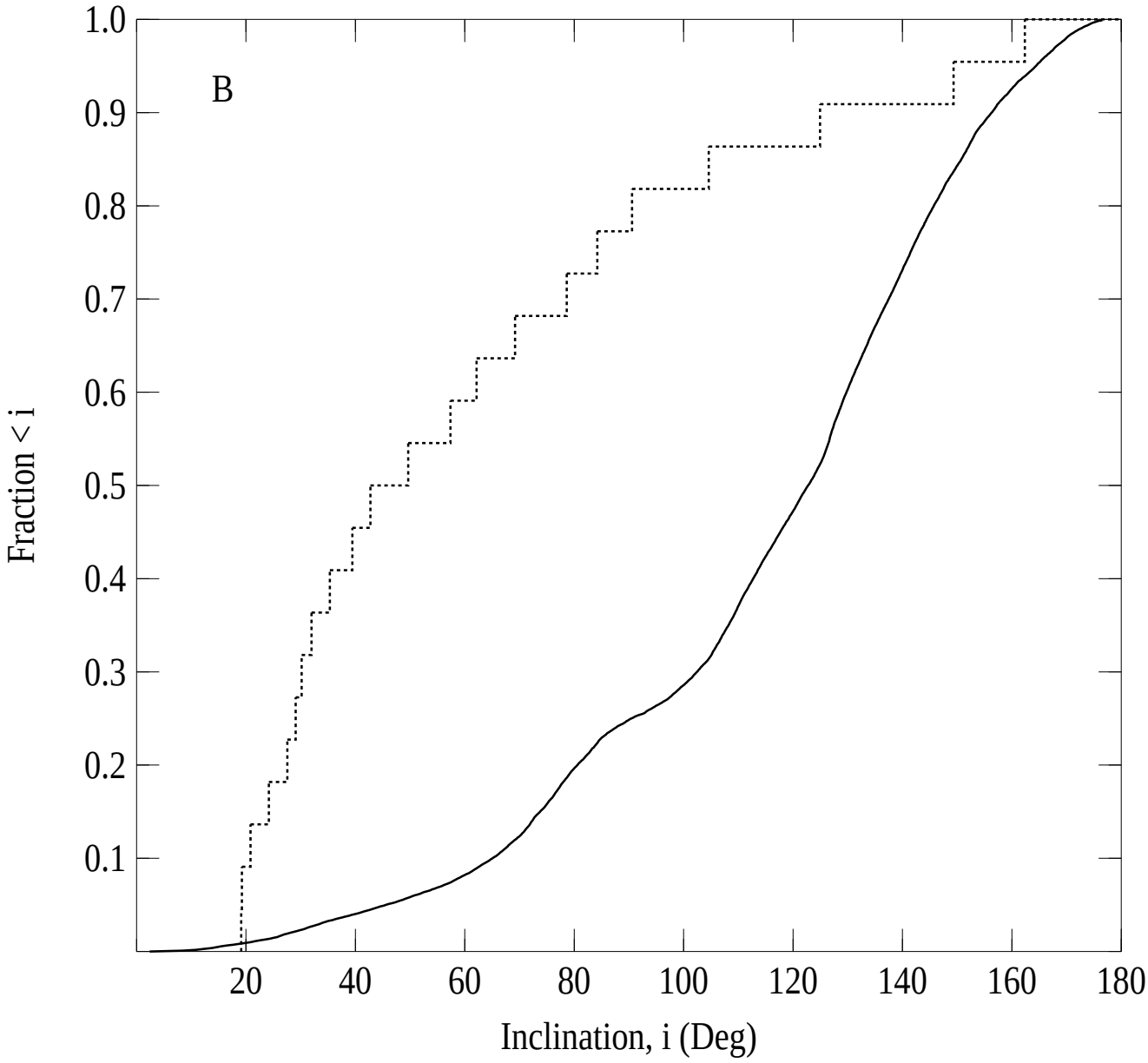
B
Fraction < i
Inclination, i (Deg)
1.0
0.9
0.8
0.7
0.6
0.5
0.4
0.3
0.2
0.1
20
40
60
80
100
120
140
160
180

Figure 5A —

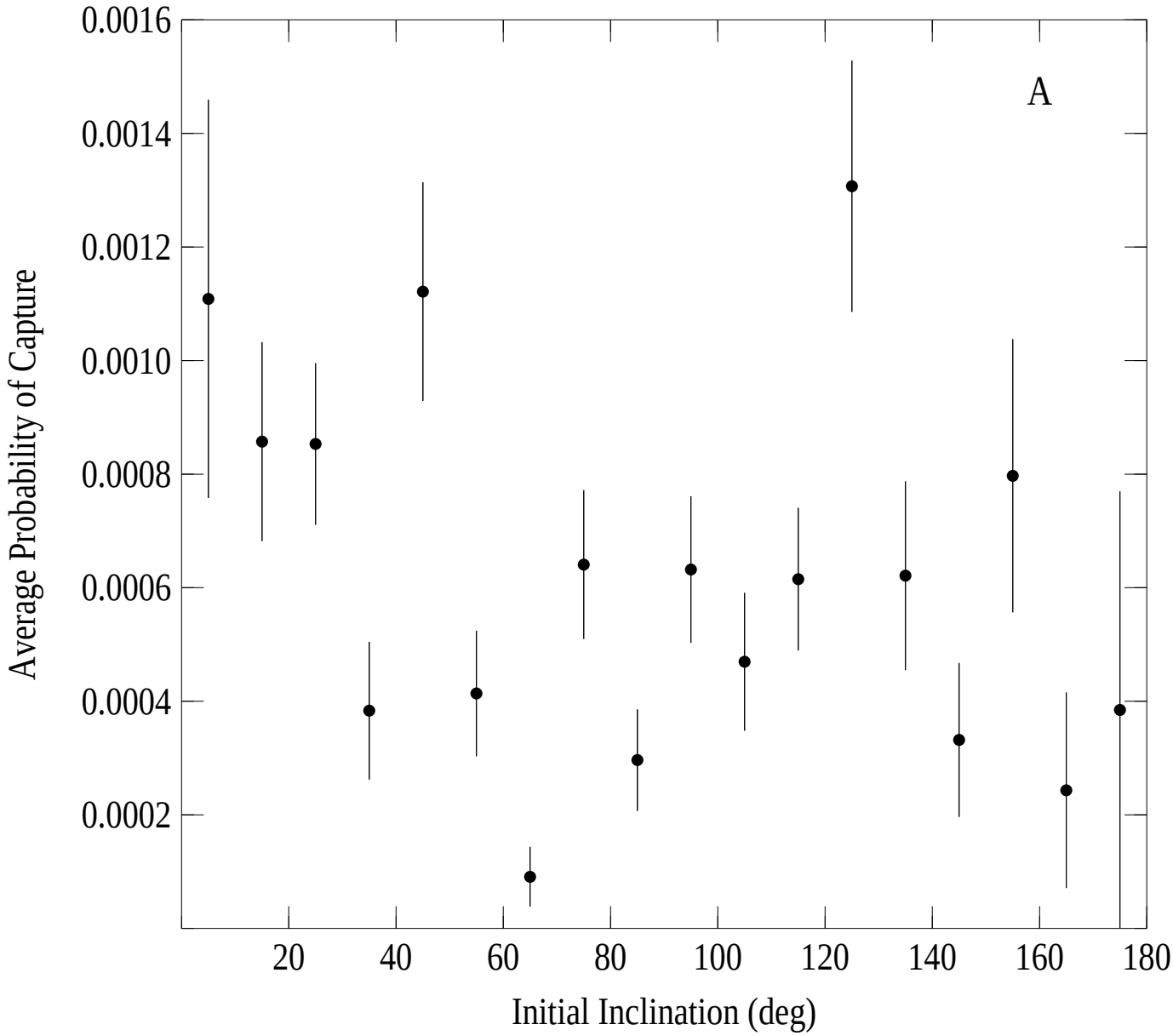

Figure 5B —

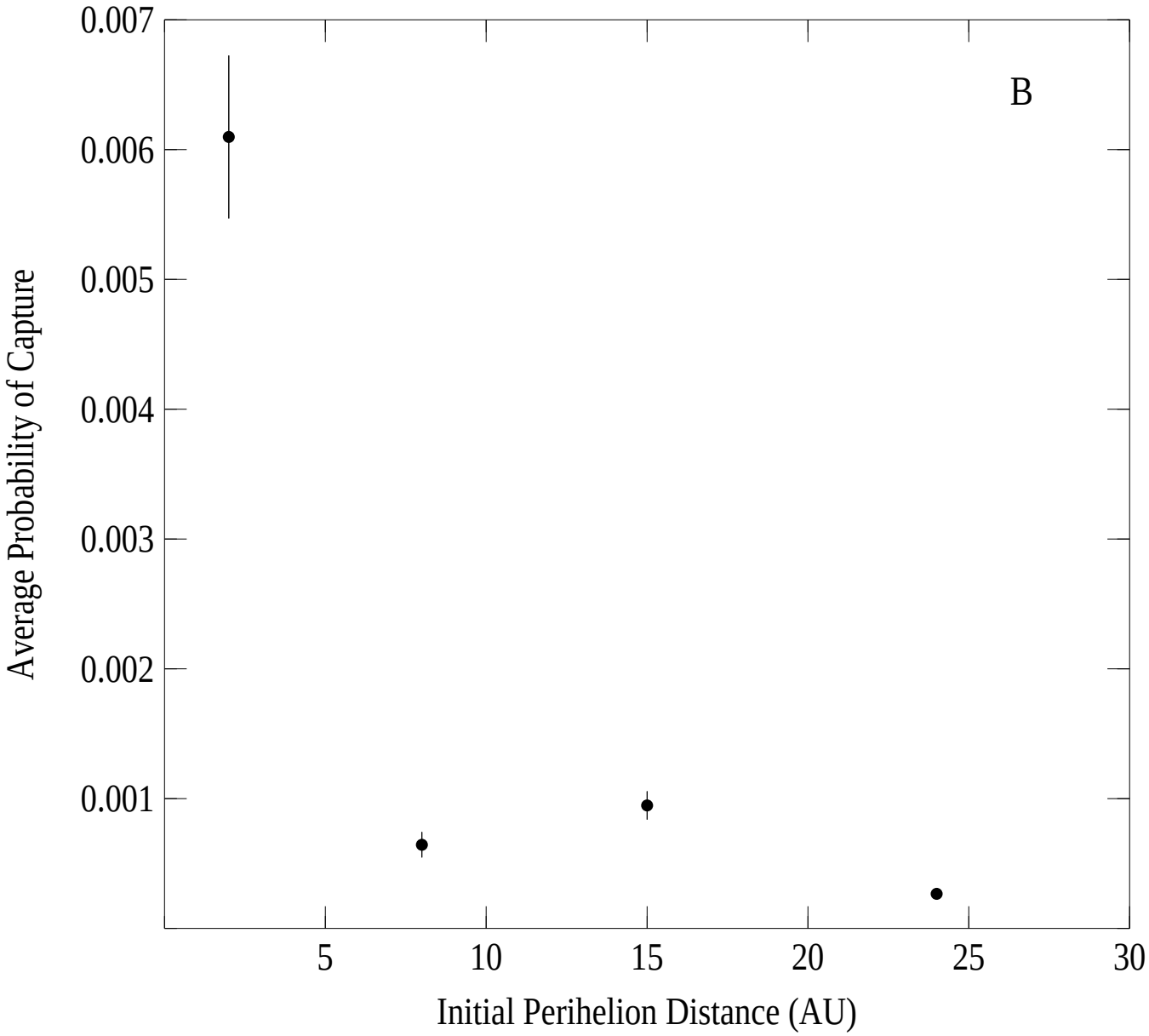
B
Average Probability of Capture
0.007
0.006
0.005
0.004
0.003
0.002
0.001
5
10
15
20
25
30
Initial Perihelion Distance (AU)

Figure 6 —

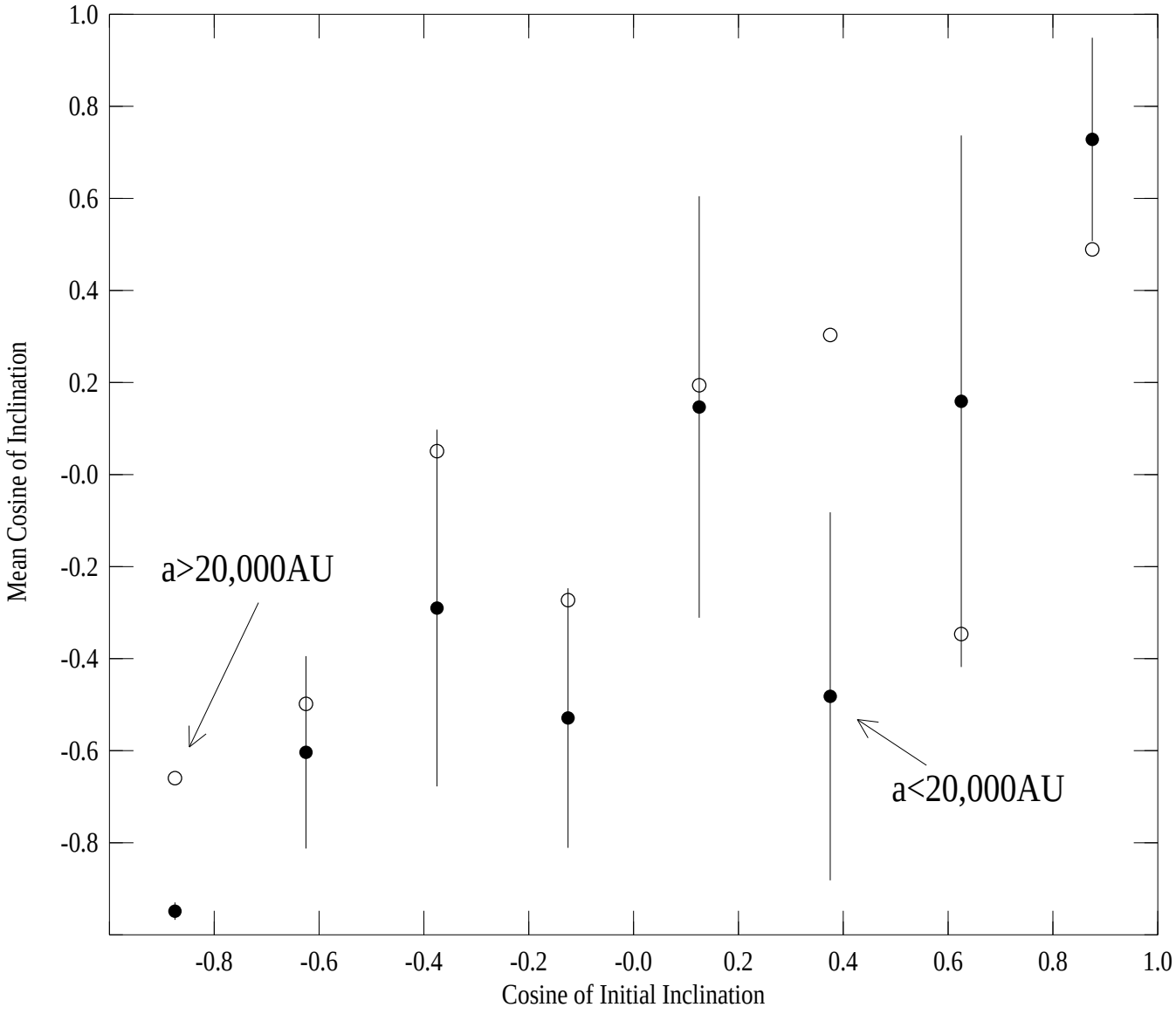
1.0
0.8
0.6
0.4
0.2
-0.0
-0.2
-0.4
-0.6
-0.8
Mean Cosine of Inclination
a>20,000AU
a<20,000AU
-0.8
-0.6
-0.4
-0.2
-0.0
0.2
0.4
0.6
0.8
1.0
Cosine of Initial Inclination

Figure 7 —

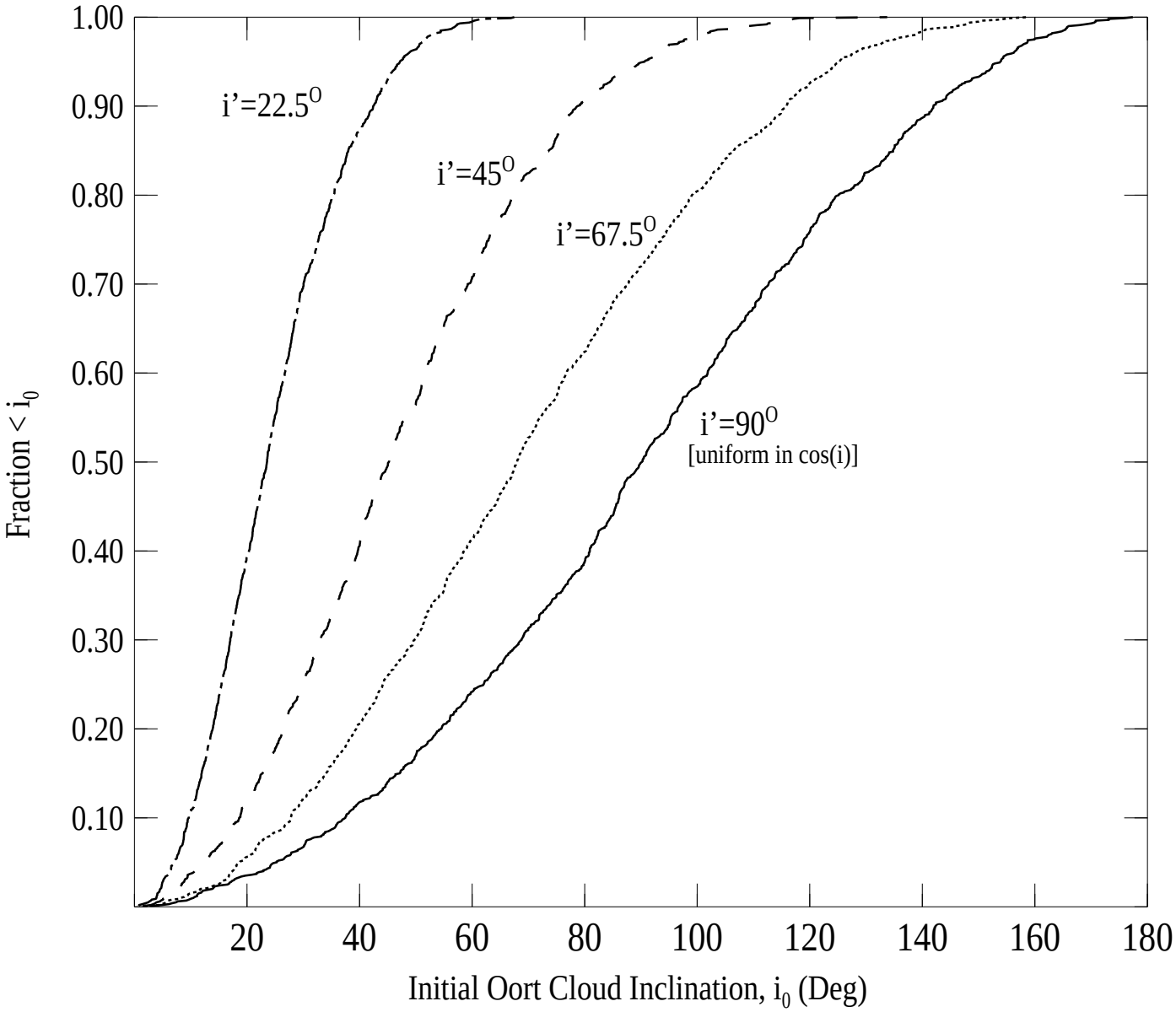
1.00
0.90
0.80
0.70
0.60
0.50
0.40
0.30
0.20
0.10
Fraction < i_0
i'=22.5^O
i'=45^O
i'=67.5^O
i'=90^O
[uniform in cos(i)]
20
40
60
80
100
120
140
160
180
Initial Oort Cloud Inclination, i_0 (Deg)

Figure 8A —

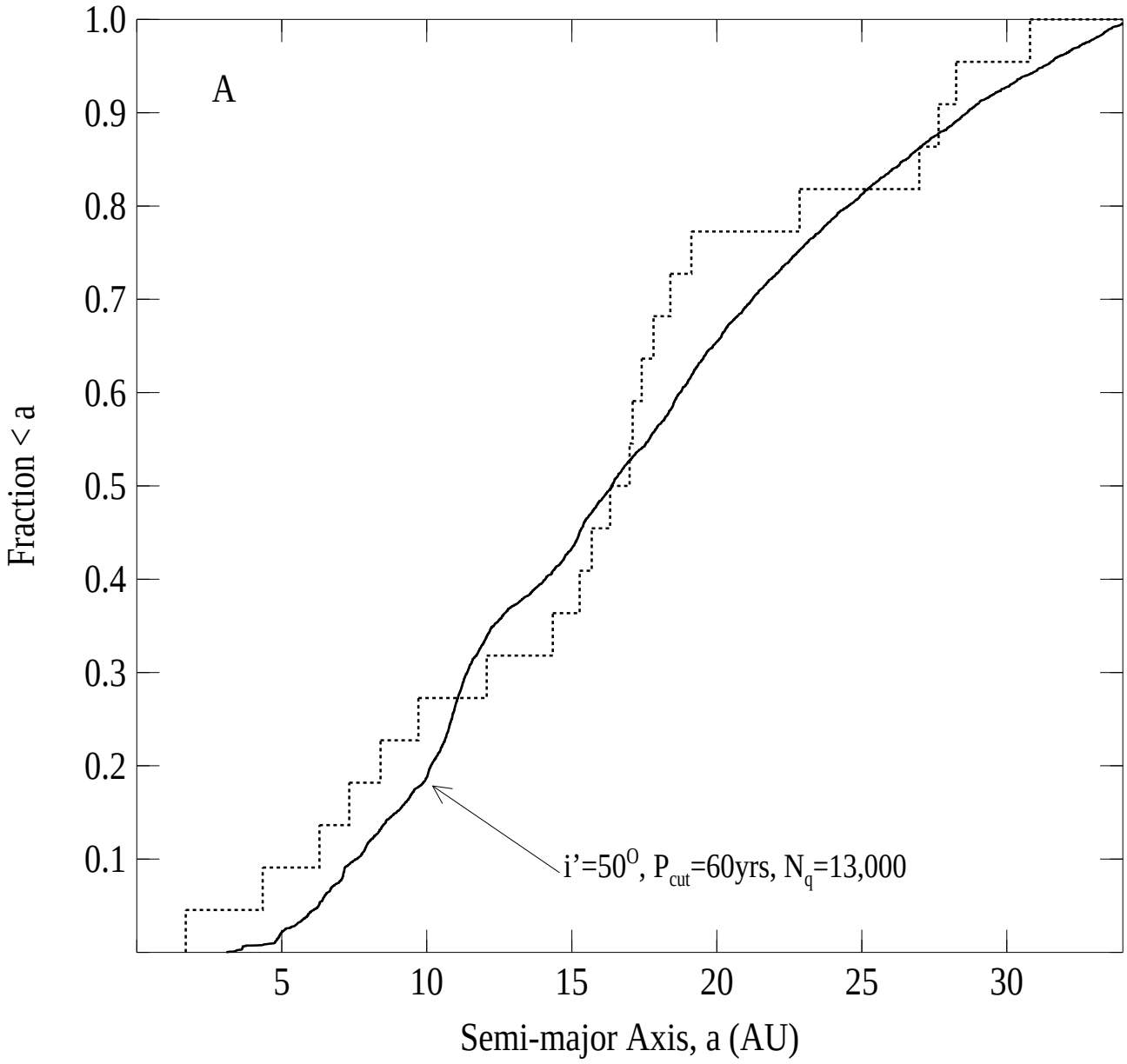
A
Fraction < a
Semi-major Axis, a (AU)
i'=50^{O}, P_{cut}=60yrs, N_q=13,000
1.0
0.9
0.8
0.7
0.6
0.5
0.4
0.3
0.2
0.1
5
10
15
20
25
30

Figure 8B —

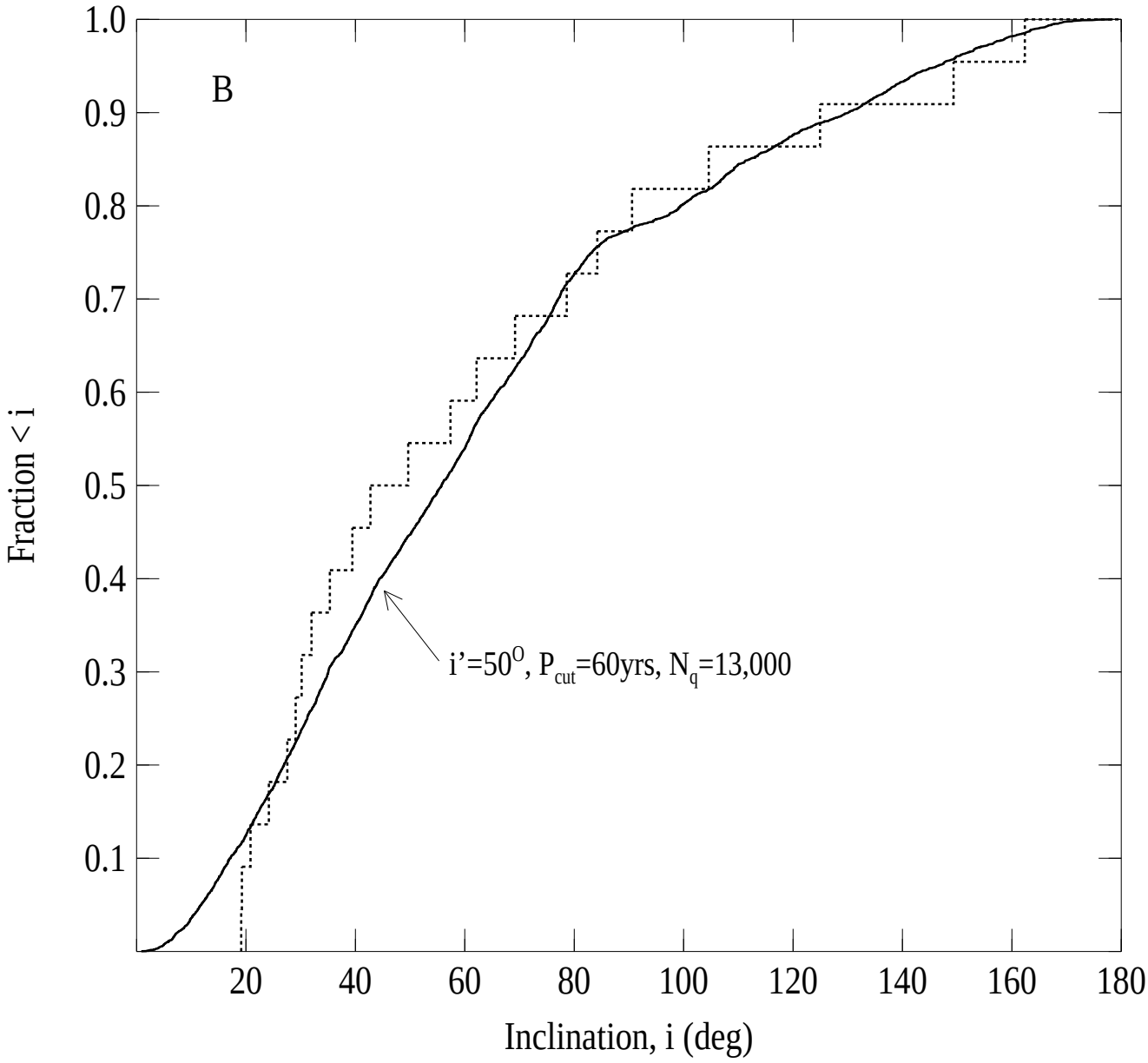
B
Fraction < i
Inclination, i (deg)
i'=50^{O}, P_{cut}=60yrs, N_q=13,000
1.0
0.9
0.8
0.7
0.6
0.5
0.4
0.3
0.2
0.1
20
40
60
80
100
120
140
160
180

Figure 9A —

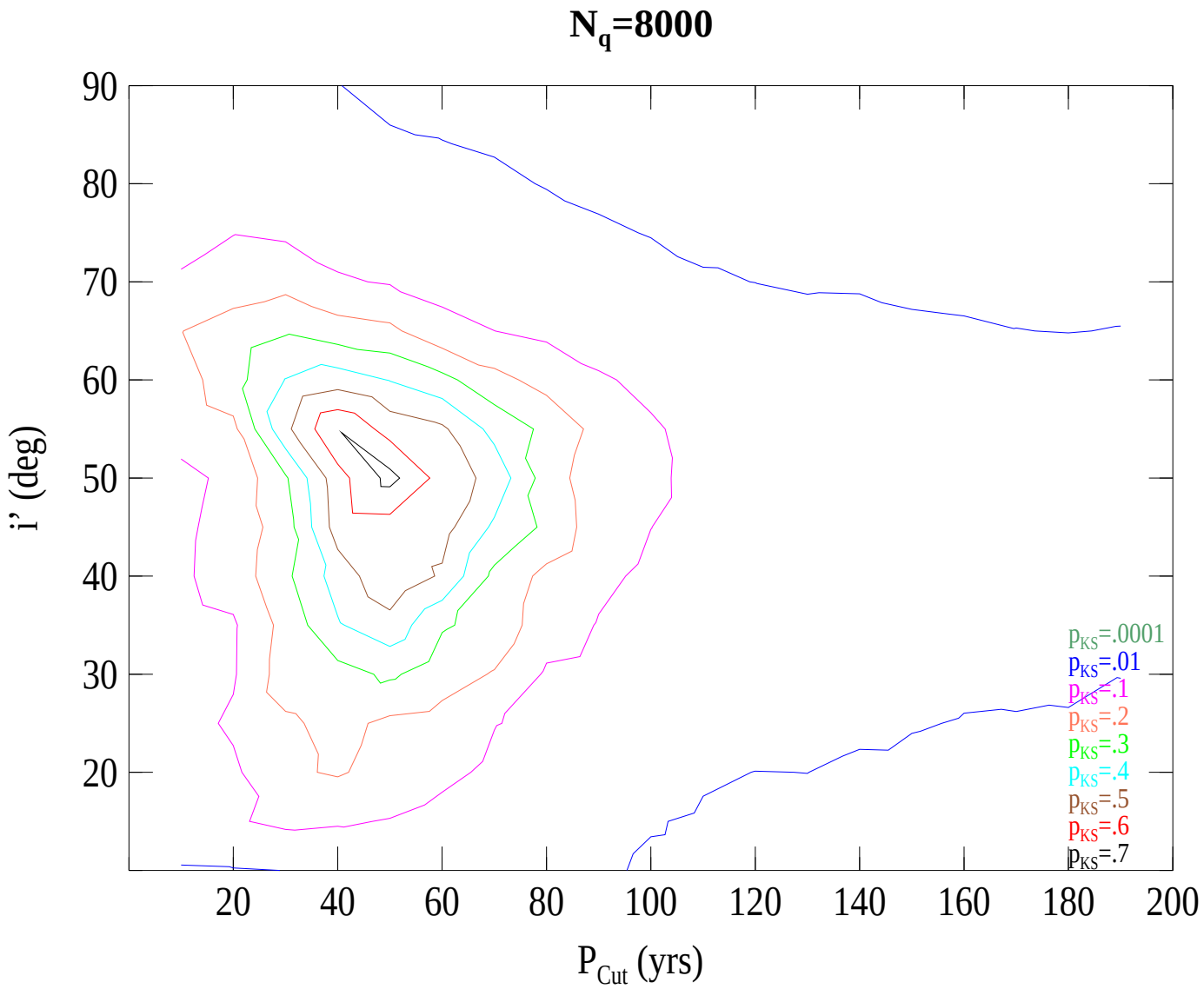
N_q=8000
i' (deg)
P_{Cut} (yrs)
p_{KS}=.0001
p_{KS}=.01
p_{KS}=.1
p_{KS}=.2
p_{KS}=.3
p_{KS}=.4
p_{KS}=.5
p_{KS}=.6
p_{KS}=.7

Figure 9B —

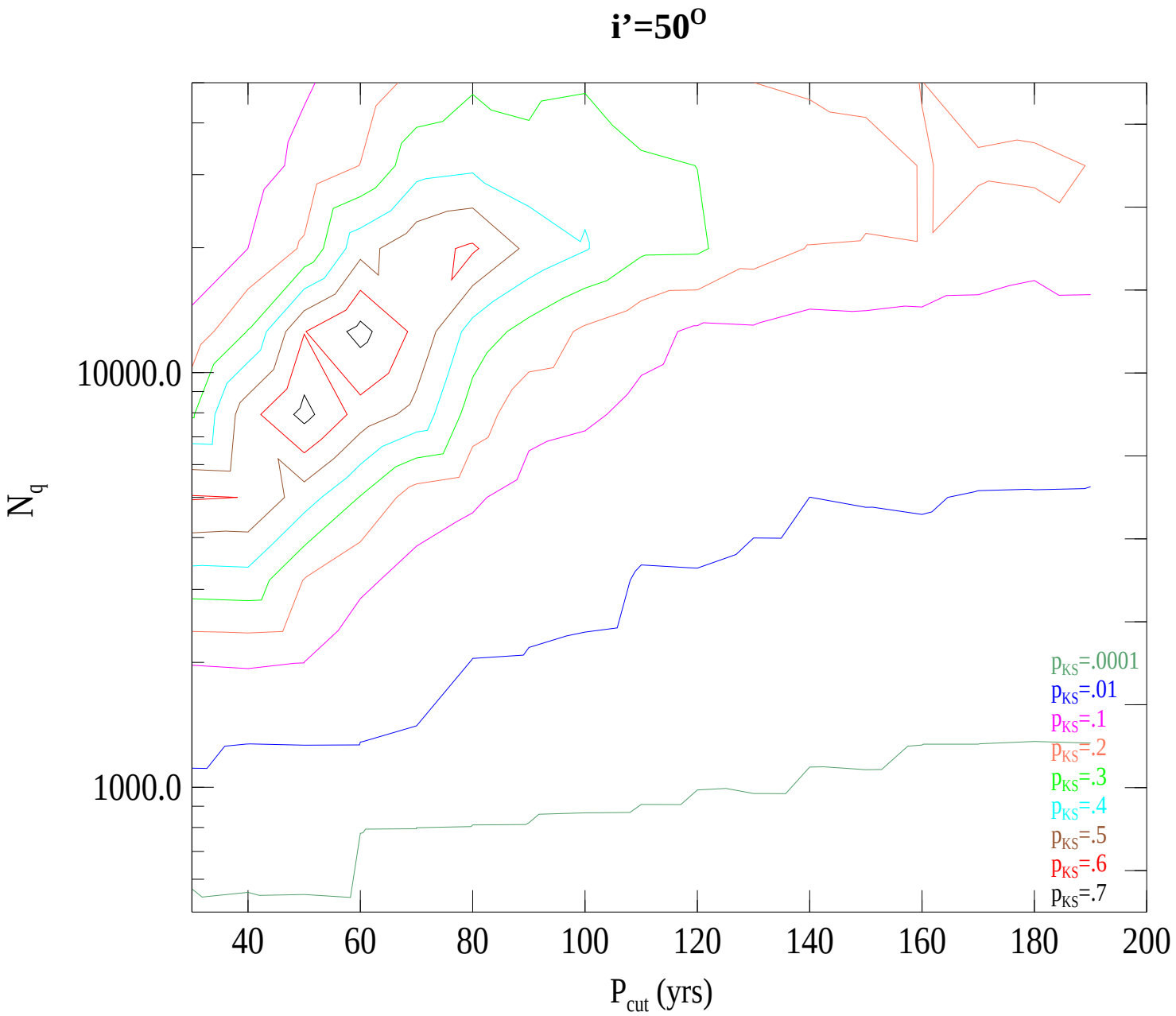
i'=50°
10000.0
1000.0
N_q
40
60
80
100
120
140
160
180
200
P_cut (yrs)
p_KS=.0001
p_KS=.01
p_KS=.1
p_KS=.2
p_KS=.3
p_KS=.4
p_KS=.5
p_KS=.6
p_KS=.7

Figure 10A —

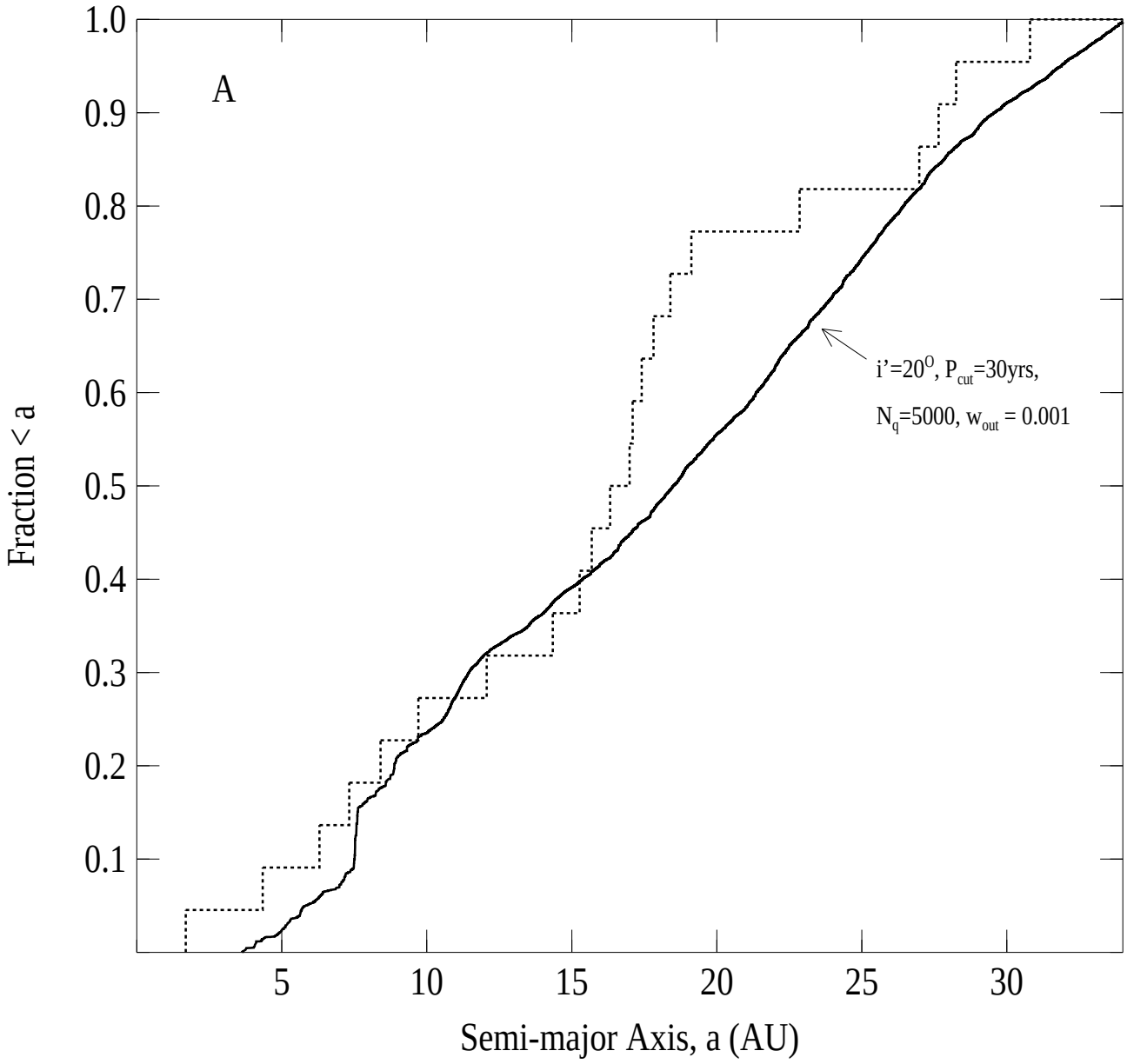
A
Fraction < a
Semi-major Axis, a (AU)
i'=20^O, P_cut=30yrs,
N_q=5000, w_out = 0.001
1.0
0.9
0.8
0.7
0.6
0.5
0.4
0.3
0.2
0.1
5
10
15
20
25
30

Figure 10B —

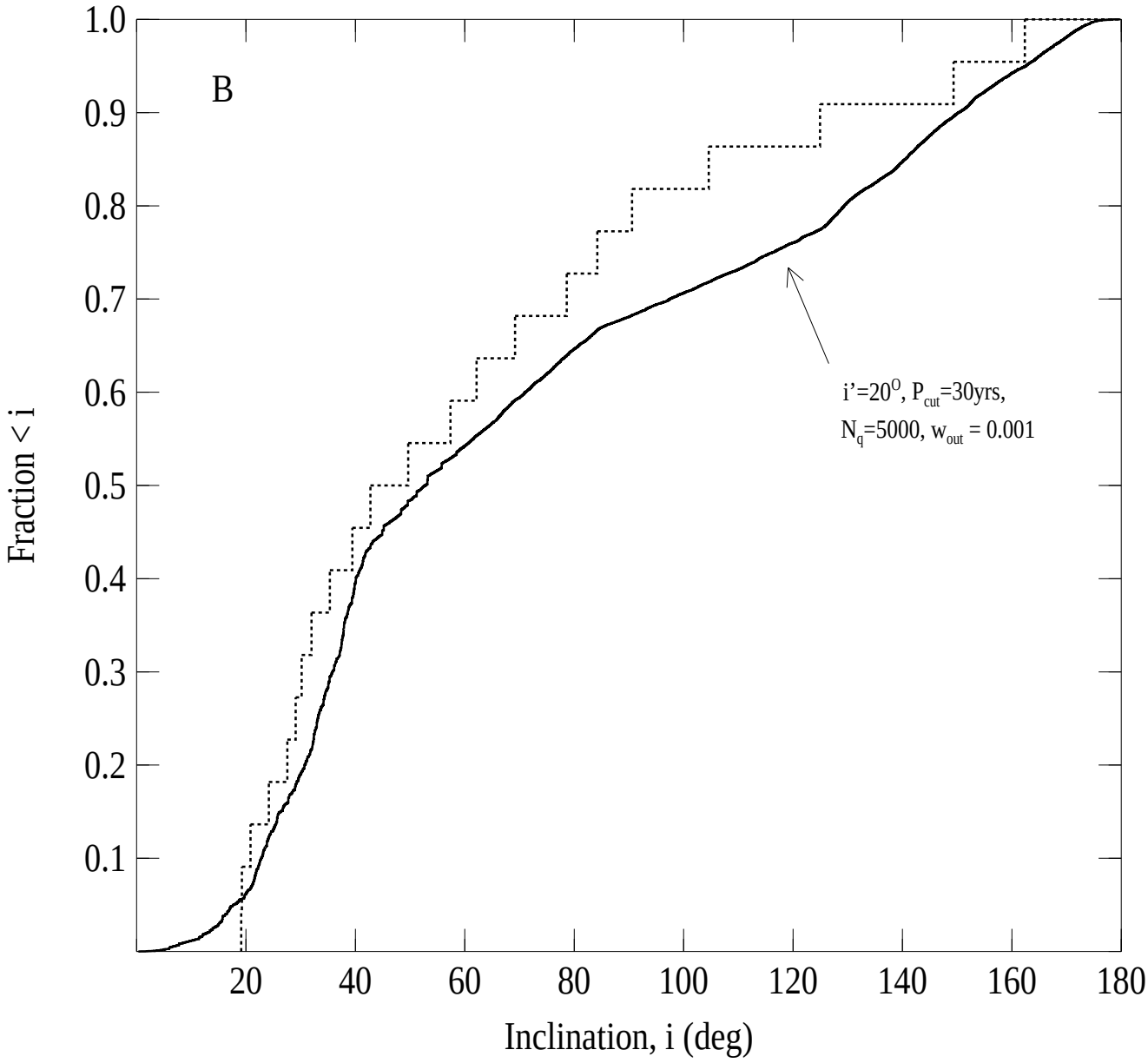
B
Fraction < i
Inclination, i (deg)
i'=20^O, P_cut=30yrs,
N_q=5000, w_out = 0.001
1.0
0.9
0.8
0.7
0.6
0.5
0.4
0.3
0.2
0.1
20
40
60
80
100
120
140
160
180

Figure 10C —

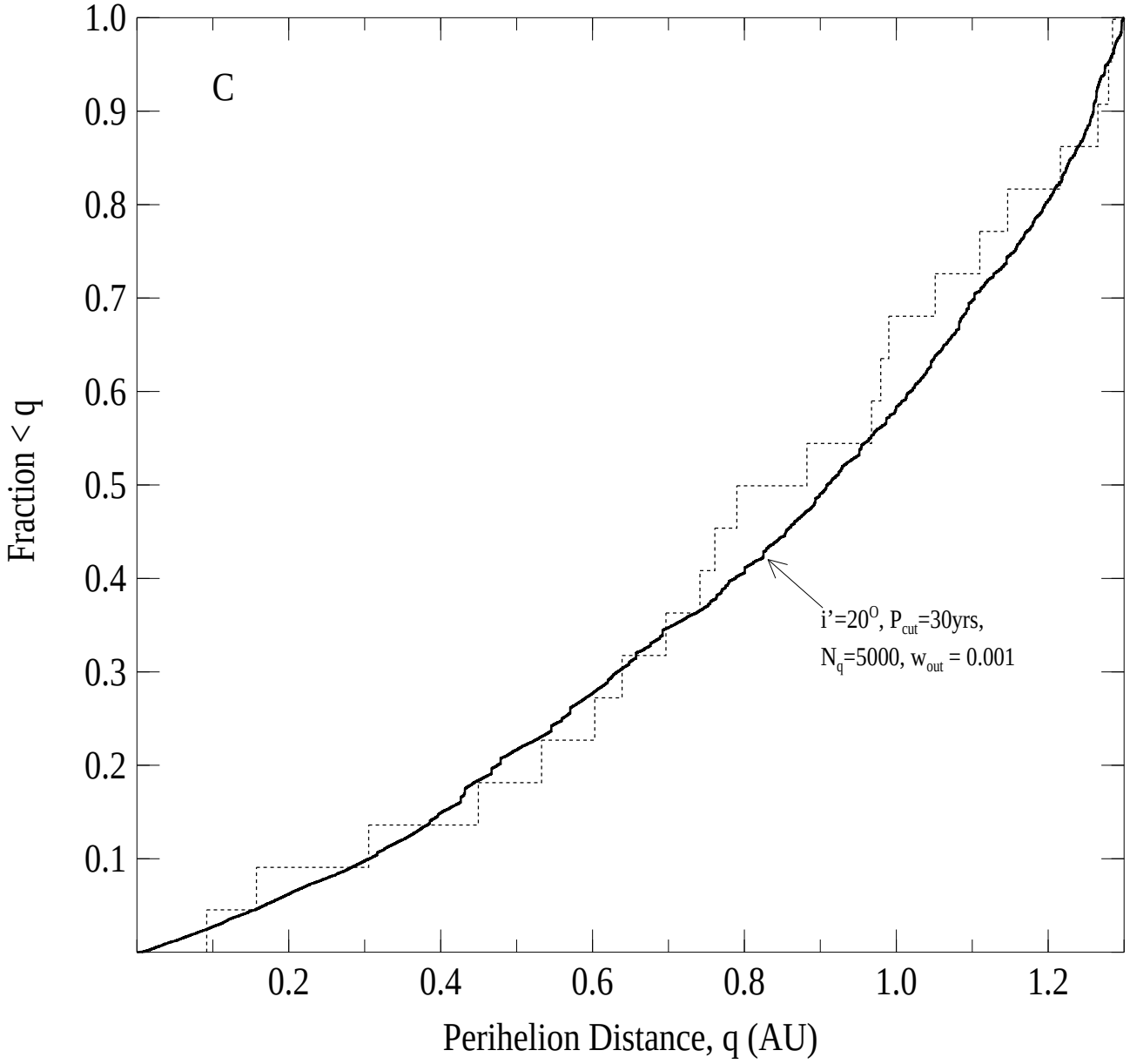
C
Fraction < q
Perihelion Distance, q (AU)
i'=20^{O}, P_{cut}=30yrs,
N_q=5000, w_{out} = 0.001
1.0
0.9
0.8
0.7
0.6
0.5
0.4
0.3
0.2
0.1
0.2
0.4
0.6
0.8
1.0
1.2

Figure 11 —

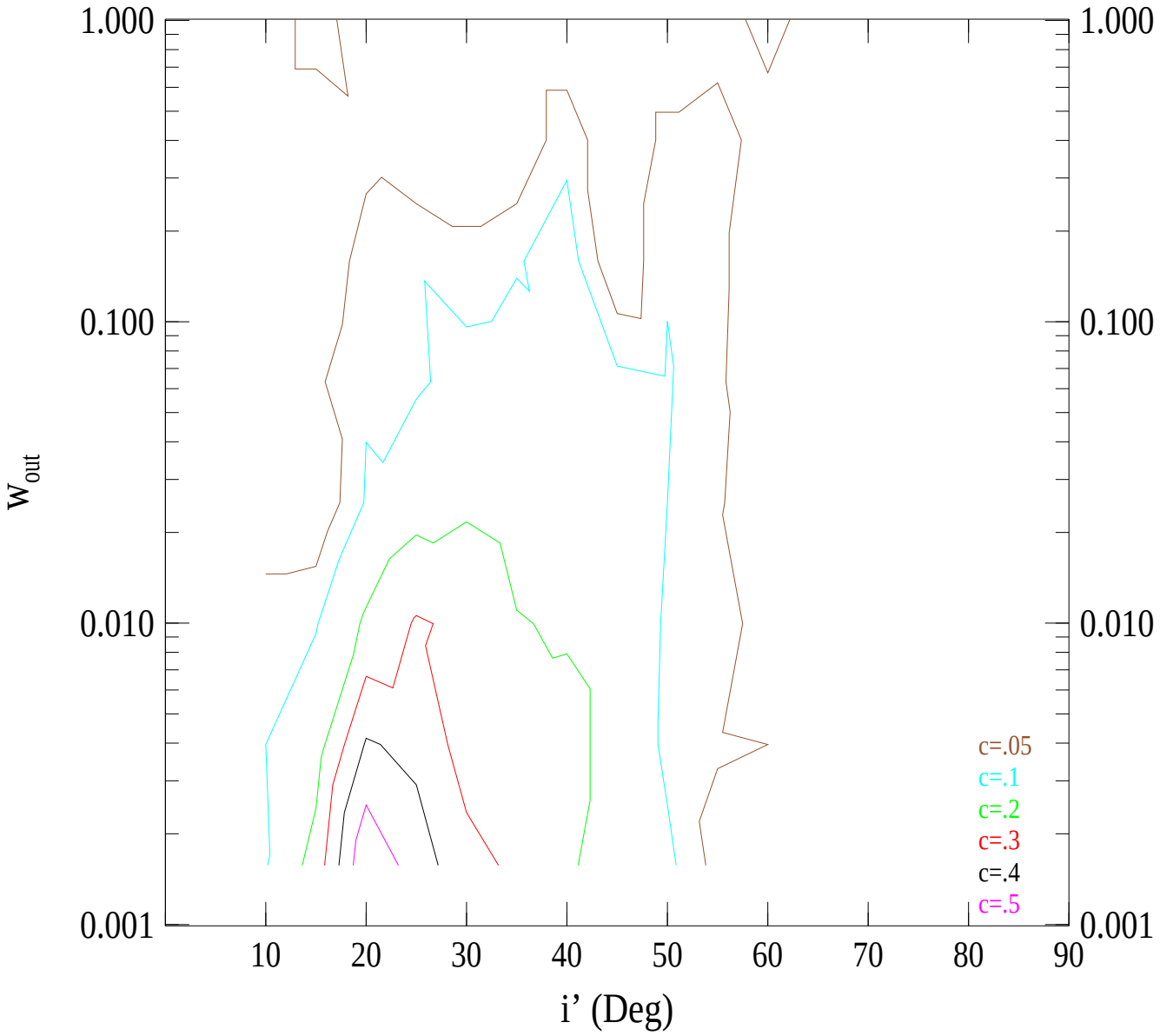
1.000
0.100
0.010
0.001
W_out
10
20
30
40
50
60
70
80
90
i' (Deg)
c=.05
c=.1
c=.2
c=.3
c=.4
c=.5

Figure 12 —

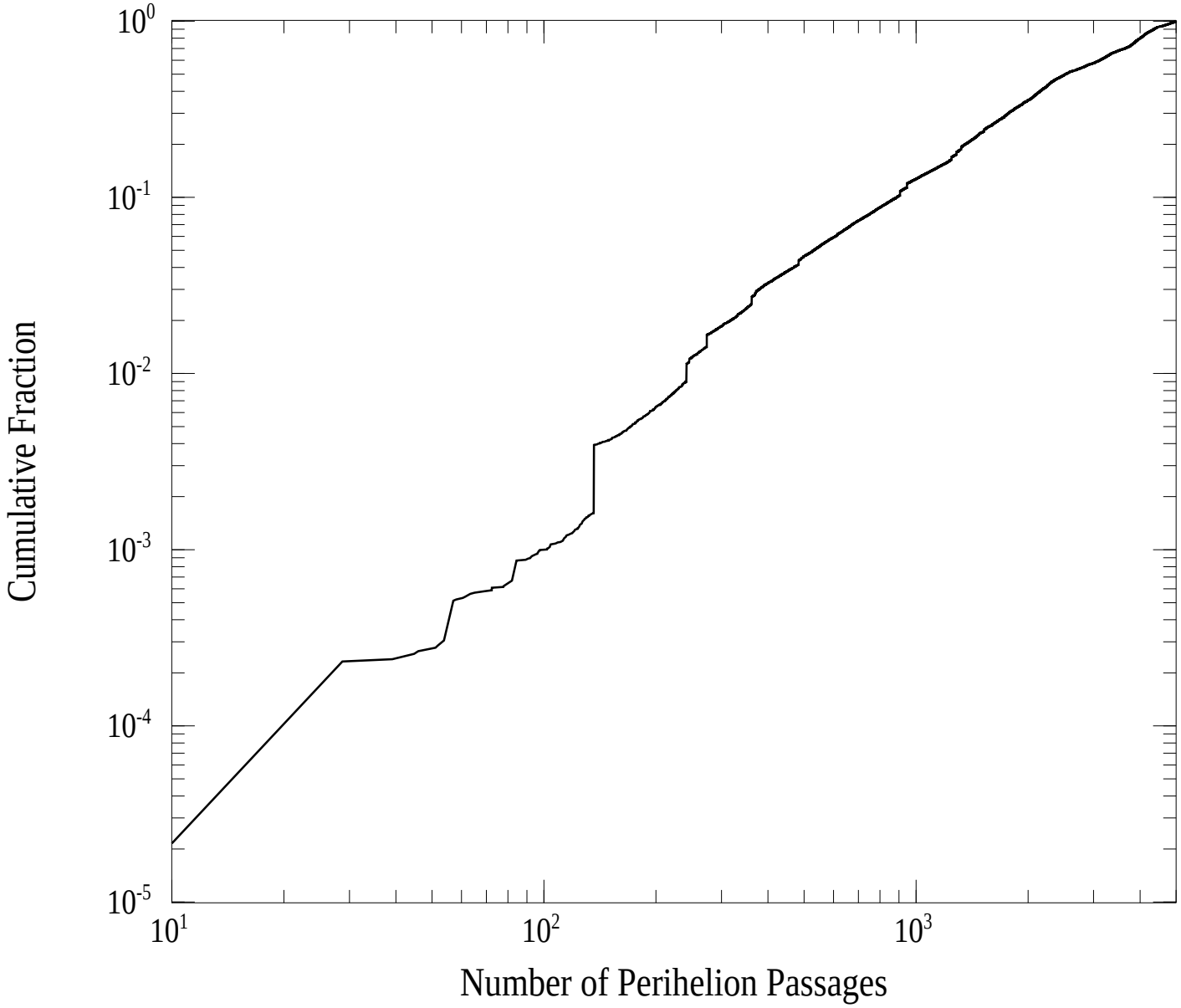
Cumulative Fraction
10^{0}
10^{-1}
10^{-2}
10^{-3}
10^{-4}
10^{-5}
10^{1}
10^{2}
10^{3}
Number of Perihelion Passages

Figure 13A —

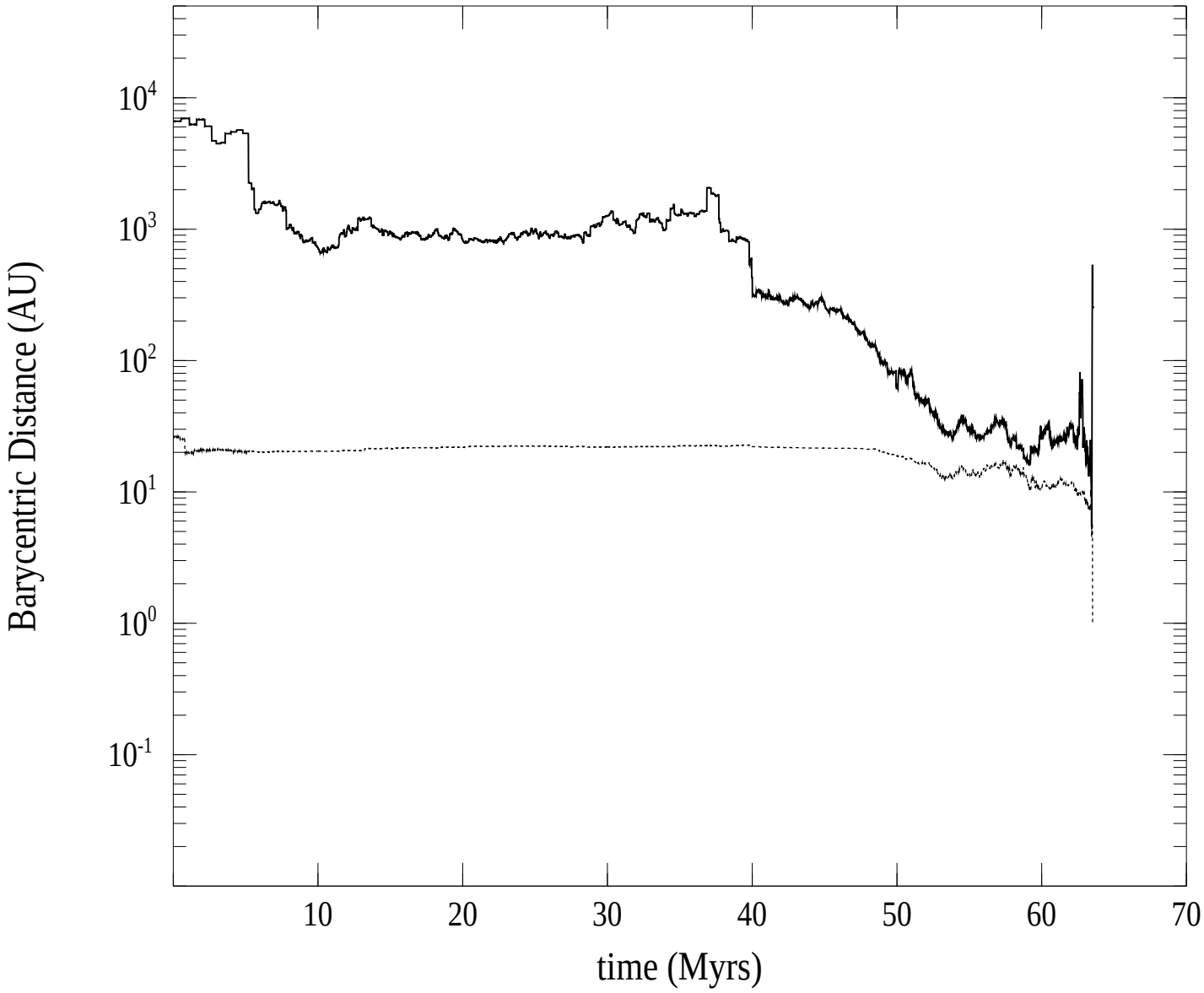
Barycentric Distance (AU)
10^4
10^3
10^2
10^1
10^0
10^{-1}
10
20
30
40
50
60
70
time (Myrs)

Figure 13B —

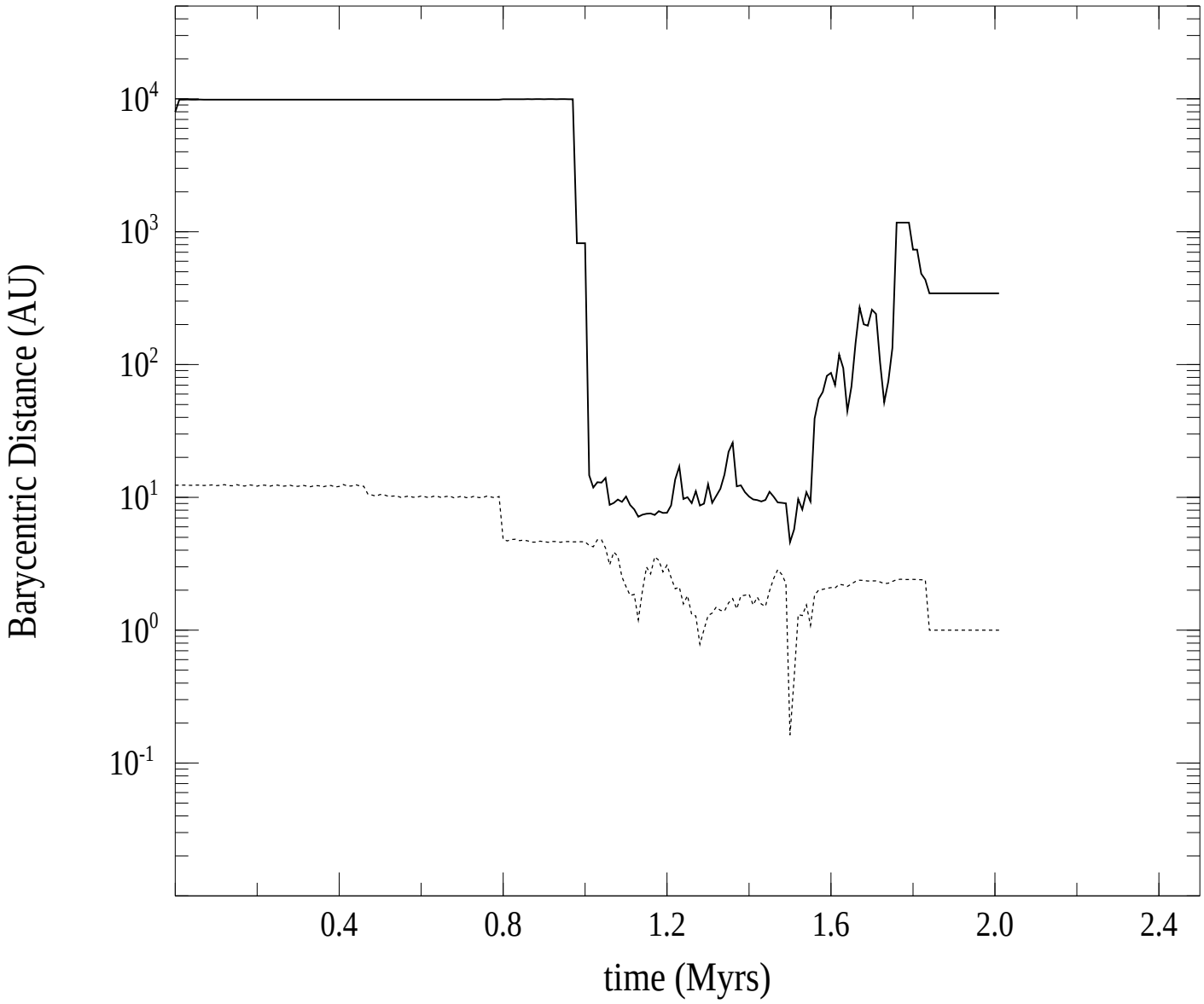
Barycentric Distance (AU)
10^4
10^3
10^2
10^1
10^0
10^{-1}
0.4
0.8
1.2
1.6
2.0
2.4
time (Myrs)

Figure 13C —

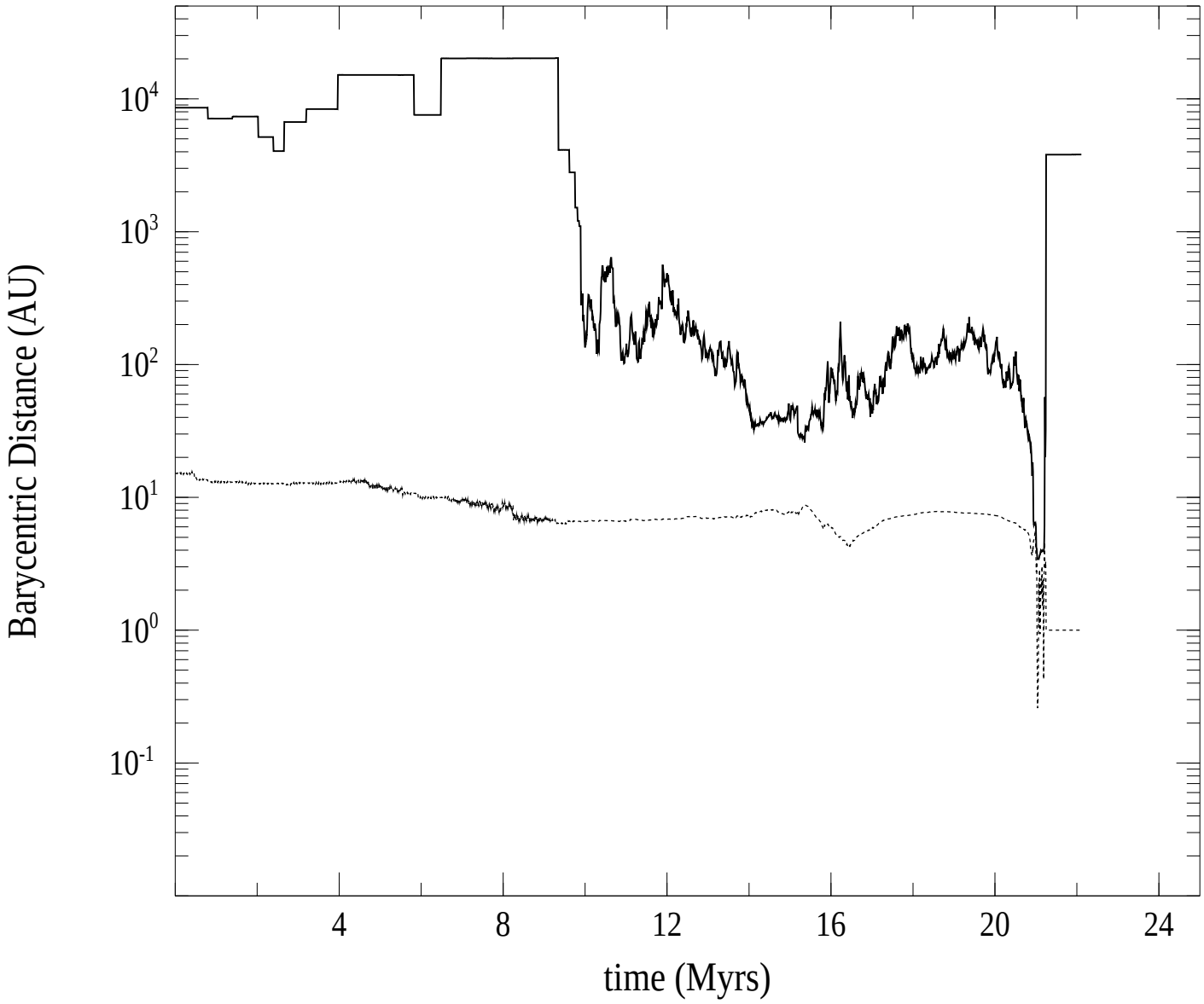
Barycentric Distance (AU)
10^4
10^3
10^2
10^1
10^0
10^{-1}
4
8
12
16
20
24
time (Myrs)

Figure 13D —

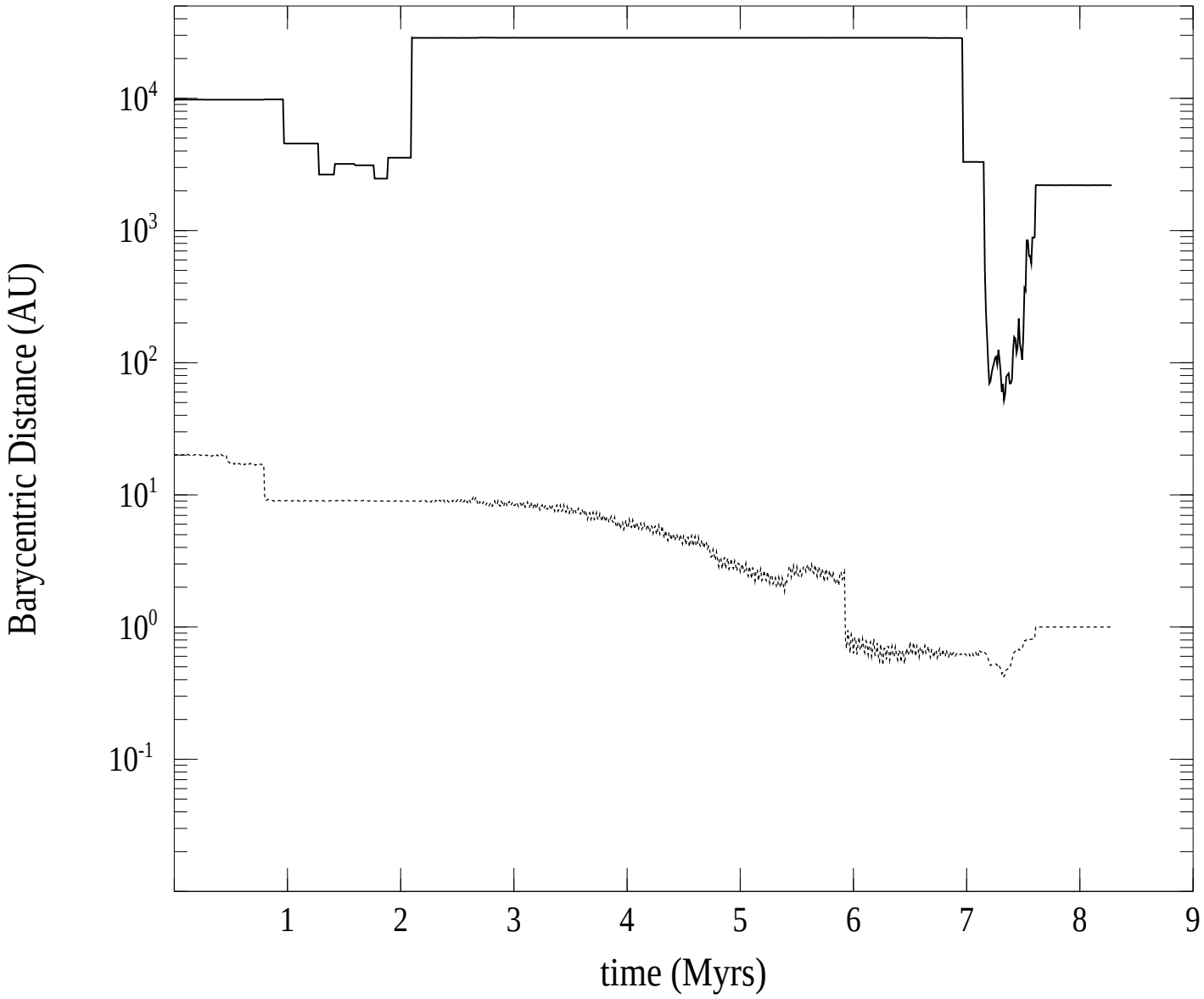
Barycentric Distance (AU)
10^4
10^3
10^2
10^1
10^0
10^{-1}
1
2
3
4
5
6
7
8
9
time (Myrs)